Dynamics of inorganic nitrogen cycling, redox conditions, and microbial community composition in a floodplain soil induced by a heavy rainfall after summer drought

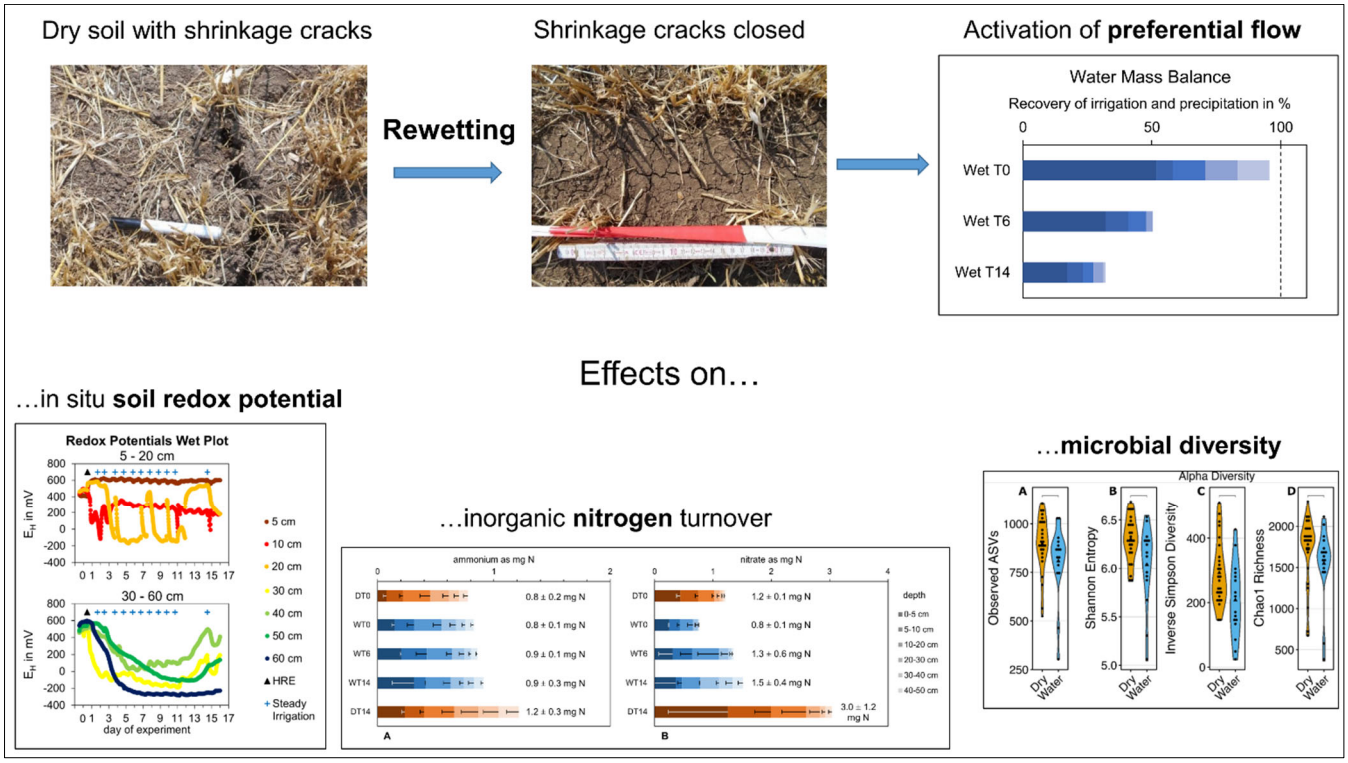
Johanna Schlögl[1], Clemens Karwautz[2], Lena Cramaro[2], Wolfgang Wanek[3], Judith Prommer[3], Theresa Böckle[3], Andreas Kappler[4], Stefan B. Haderlein[1], Christian Griebler[2]

[1]Environmental Mineralogy, Department of Geosciences, University of Tübingen, Schnarrenbergstraße 94-96, 72076 Tübingen, Germany
[2]Department of Functional and Evolutionary Ecology, Division of Limnology, University of Vienna, Djerassiplatz 1, 1030 Vienna, Austria
[3]Division of Terrestrial Ecosystem Research, Department of Microbiology and Ecosystem Science, Center of Microbiology and Environmental Systems Science, University of Vienna, Djerassiplatz 1, 1030 Vienna, Austria
[4]Geomicrobiology, Department of Geosciences, University of Tübingen, Schnarrenbergstraße 94-96, 72076 Tübingen, Germany

Correspondence to: Christian Griebler (christian.griebler@univie.ac.at), Stefan B. Haderlein (stefan.haderlein@uni-tuebingen.de)

Abstract. Climate change ~~increases~~is increasing the frequency of droughts ~~and~~followed by heavy rainfall ~~events~~ in temperate ~~climates~~regions ~~of Central Europe. This study examined the impacts of such extreme weather events on the downward~~ , with ~~potential~~important consequences for ~~preferential~~water flow, nitrogen transport ~~of water and inorganic nitrogen species, the main processes governing inorganic nitrogen turnover and the~~ , redox dynamics ~~of the soil~~, and microbial ~~community~~activity in ~~loamy~~ floodplain soils. ~~To this end, we conducted~~ We investigated these coupled responses in a field experiment ~~simulating~~on a fine-textured arable Gleysol after ~~a~~ prolonged summer drought. A simulated heavy rainfall event ~~applying~~was applied using ~~isotopically (^{2}H) enriched~~ D_2O-labeled water ~~on a plot of arable land with fine-textured soil after a prolonged dry period. Subsequently the experimental plots were irrigated (^2H_2O)~~ as a hydrological tracer, followed by recurrent moderate irrigation with non-~~labelled~~labeled water. ~~50 cm deep soil~~ Soil cores to 50 cm depth were collected from irrigated and dry control plots ~~at different time points (~~on ~~days 0, 6/8, and 14)~~over 14 days and ~~analysed~~analyzed for soil ~~nitrate and ammonium~~ water content, ~~soil water content, ^{2}H~~ δ^2H signatures~~enrichment of soil water~~, nitrate and ammonium masses, ~~microbial~~ bacterial community composition based on DNA and RNA, ~~as well as~~and extracellular enzyme activities. ~~Furthermore,~~In situ redox potentials were ~~recorded in situ~~monitored along the soil profile ~~on dry and irrigated plots. Whereas the irrigation water of~~ . Within two hours after the simulated heavy rainfall ~~event~~, ~~labelled~~labeled ~~irrigation~~ water had ~~penetrated~~ ~~to~~reached at least 50 cm ~~deep into the soil along~~depth, indicating rapid preferential flow ~~paths after only two hours~~through drought-induced shrinkage cracks. ~~Despite this deep water infiltration, ammonium and~~ This was accompanied by a significant decline in nitrate ~~values~~mass in the topsoil without nitrate accumulation ~~masses did not increase~~ at 50 cm depth, suggesting nitrate ~~whereas nitrate declined significantly in the topsoil. This pattern suggests rapid nitrate~~ transport ~~beyond~~below the investigated profile. ~~soil depth, while~~ In contrast, ammonium remained ~~constant at 50 cm depth despite a significant decrease of nitrate in the topsoil after irrigation. This suggests that some nitrate might have been transported rapidly below 50 cm depth in contrast to ammonium, which is rather immobile in soils due to strong~~ largely retained ~~in the soil profile, most likely because of~~ sorption ~~to clay minerals. Ammonium behaved very conservatively and only~~ and increased ~~significantly~~only in the ~~topsoil~~uppermost soil layer ~~(0–5 cm) in response to the wetting of the dry soil (“)~~, consistent with a short-term rewetting-induced mineralization pulse~~, i.e. the Birch effect”). At day 6 and day 14 of the experiment, the non-labelled~~labeled ~~irrigation water of the daily recurrent~~. ~~During~~ Ssubsequent moderate irrigation ~~doses resided, most newly added water remained~~ was retained mainly in the topsoil ~~layer (0–5 cm depth), and only a small fraction penetrated to the subsoil,~~reached deeper layers, likely because ~~the~~

shrinkage cracks present at the beginning of the experiment had closed. In parallel, the in situ redox potential dropped after initial wetting. Redox potentials declined from >oxidizing conditions (> +400 mV to below) to strongly reducing conditions (< −100 mV relative tovs. the standard hydrogen electrode. Soil nitrate contents decreased when redox potentials were below +100 mV and vice versa. This implies that nitrate formation and transformation after the initial rewetting was governed by soil redox conditions instead of processes induced by the rewetting after drought.)declined after irrigation, and were associated with later changes in nitrate pools, although with pronounced temporal and depth-dependent variability. Nitrate masses tended to decrease under low redox potentials and increase when redox potentials recovered, indicating that redox conditions likely contributed to nitrate dynamics after the initial rewetting phase. However, because nitrogen transformation rates were not directly measured. , these patterns should be interpreted as evidence for redox-associated changes in inorganic nitrogen pools rather than direct process-rate estimates. Microbial Bacterial community composition remained stable at both DNA and RNA levels, whereas analysis showed no significant differences between the active fraction of the community (RNA) on irrigated and dry plots.treatment effects at either the DNA or RNA level over the 14-day experiment. Diversity indices onof the RNA-levelactive community were somewhat higher on dry than on wet plots, althoughslightly, but not significantly, which suggests that drying and the following rewetting selected for more adapted taxa. In contrast, activities of the extracellular enzymes higher in dry than in irrigated soils. In contrast, β-glucosidase and exochitinase showedactivities increased after irrigation.were significantly higher activities on wet plotsin irrigated than onin dry plots, whereas the activity of acid phosphatase activity did not respond to the irrigation treatment. All enzymes decreased in activity; all enzyme activities declined with soil depth. Overall, the our results show that heavy rainfall after droughtevent had only a minor effect on the turnover of inorganic nitrogen species. Nitrogen turnover was mainly governed by redox conditions. The presence of pronounced shrinkage cracks formed after a drought period before the heavy rainfall event, however, allows forean trigger rapid created a short hydrological window for rapid nitrate displacement through preferential flow pathways, transport of nitrate dissipation into the subsoilthrough fine-textured floodplain soils, potentially bypassing nitrogen retention in the biologically active topsoil and eventuallyincreasing the risk of nitrate transfer to the underlying aquifer. Our study also showed that thedeeper soil layers or shallow groundwater. In contrast, microbial community in temperate climates reacts in terms of activity and may ultimately be reshapedcomposition remained comparatively stable over the short observation period, while extracellular enzyme activities responded rapidly to represent more resilient taxa regarding drying and rewetting cycles. .



1 Introduction

Floodplains are biogeochemically active interfaces between terrestrial and aquatic systems and play an important ~~landscape compartments when it comes to~~ role in nitrogen retention and turnover ~~(Lair et al., 2009; Venterink et al., 2003). Often, floodplain soils are~~ (Lair et al., 2009; Venterink et al., 2003). Their soils are often exposed to recurrent inundation ~~and dry periods, or they are influenced by alternating~~, drying, and fluctuations in groundwater ~~levels throughout the year (Baldwin and Mitchell, 2000; Coby et al., 2011). In both cases, they experience alternating~~ level, which cause pronounced shifts in oxygen availability and ~~thus fluctuating~~ redox conditions~~. The availability of oxygen determines which nitrogen turnover processes dominate (Baldwin and Mitchell, 2000; Hefting et al., 2004). Inorganic nitrogen in the form of ammonium is released during the mineralization of organic matter. Ammonium is relatively stable~~ (Baldwin and Mitchell, 2000; Coby et al., 2011). These redox fluctuations regulate the dominant pathways of inorganic nitrogen transformation (Baldwin and Mitchell, 2000; Hefting et al., 2004). Organic matter mineralization releases ammonium, which may accumulate under reducing conditions ~~but is nitrified~~or be oxidized to nitrate under ~~oxidizing~~oxic conditions. ~~Under reducing~~ Conversely, nitrate is reduced under low-oxygen conditions, ~~nitrate is~~ mainly ~~denitrified~~through denitrification to ~~N_2O~~N_2O and ~~N_2~~N_2 via nitrite and ~~NO.~~ nitric oxide. Thus, floodplain soils are hotspots of nitrogen transformation, but the balance between nitrogen retention, gaseous loss, and leaching depends strongly on hydrological connectivity and redox dynamics.

~~Climate change increases the frequency and amplitude of weather extremes such as drought periods and heavy rainfall events (Coumou and Rahmstorf, 2012; Horton et al., 2016; Perkins et al., 2012). Heavy rainfall after summer drought triggers important hydrological and biogeochemical processes, particularly in fine-textured, loamy soils. First of all, drought causes the formation of shrinkage cracks of substantial width and depth, that allow for preferential flow (Beven and Germann, 2013; Jarvis et al., 2016; Nimmo, 2021) and thereby fast vertical solute and particle-bound transport of nutrients and agrochemicals (Bronswijk et al., 1995; Kelly and Pomes, 1998; Schlögl et al., 2022) during a following heavy rainfall event. The two inorganic nitrogen species ammonium and nitrate differ strongly in their chemistry and biogeochemical behaviour in soils. Ammonium as a cation is prone to sorption to the mostly negatively charged soil mineral particles whereas nitrate as an anion is little sorbed in soils and therefore more mobile in pore water (Blume et al., 2016) and can thus be lost from the soil system by leaching. The fate of ammonium and nitrate during rewetting of dry soils is also determined by the so-called Birch effect. This effect~~

~~describes the occurrence of a temporary flush of inorganic nitrogen after the rewetting of dry soil, that was observed in both lab (Birch, 1958, 1960) and field experiments (Cui and Caldwell, 1997). This flush of inorganic nitrogen is caused by microbial lysis, mineralization of dead microbial biomass, and by decomposition of osmoregulatory substances released by microorganisms upon rewetting (Fierer and Schimel, 2002; Jarvis et al., 2007; Saetre and Stark, 2005; Unger et al., 2010). The effect can last up to several days in the field with the main fraction of nitrogen mineralized in the first three days after wetting (Cui and Caldwell, 1997). Despite the potential importance of the Birch effect on inorganic soil nitrogen cycling, it is only triggered by severe drying-rewetting cycles. After this pulse of nitrogen seizes it is later expected that the "usual" redox-driven processes dominate soil inorganic nitrogen cycling, including mineralization, nitrification and denitrification.~~

~~Inorganic nitrogen turnover processes are largely microbiologically driven in soils. The soil microbial community adapts to regular drying and rewetting cycles (Armstrong et al., 2016; Fierer et al., 2003; Veach and Zeglin, 2020). Dependent on the frequency and intensity of the disturbance in hydraulic and redox conditions, dynamics of microbial community composition and activities may respond differently (Moche et al., 2015; Rinklebe et al., 2006). In mid-European temperate climates such as at our study site, drying and rewetting cycles might become more frequent in the future due to climate change (Coumou and Rahmstorf, 2012; Horton et al., 2016; Perkins et al., 2012). It is therefore important to understand their effects on microbial community activity and composition and related changes in soil nitrogen cycling.~~

~~The objectives of our study were (i) to evaluate the water flow and solute transport during a drying-rewetting event induced by heavy rainfall following a summer drought~~ Climate change is expected to increase the frequency and intensity of weather extremes, including droughts and heavy rainfall events, in temperate regions of Central Europe (Coumou and Rahmstorf, 2012; Horton et al., 2016; Perkins et al., 2012). Heavy rainfall following summer drought can trigger rapid hydrological and biogeochemical responses, particularly in fine-textured, loamy soils. During drought, shrinkage cracks may form and create preferential flow paths that allow water, dissolved solutes, and particle-associated compounds to bypass much of the soil matrix and move rapidly into deeper soil layers (Beven and Germann, 2013; Jarvis et al., 2016; Nimmo, 2021). Such preferential flow has been shown to enhance the vertical transport of nutrients and agrochemicals during subsequent rainfall events (Bronswijk et al., 1995; Kelly and Pomes, 1998; Schlögl et al., 2022). For inorganic nitrogen, this process is particularly relevant because ammonium and nitrate differ strongly in mobility. Ammonium is retained by sorption to negatively charged mineral surfaces, especially clay minerals, whereas nitrate is weakly sorbed and can therefore be transported with percolating and infiltrating water (Blume et al., 2016). Heavy rainfall after drought may therefore decouple the vertical redistribution of water, nitrate, and ammonium, with potential implications for nitrogen retention in the soil profile and nitrate transfer to deeper soil layers or groundwater.

In addition to physical transport, rewetting of dry soil can stimulate short-lived pulses of microbial activity and nitrogen mineralization, commonly referred to as the Birch effect. This effect describes the transient release of inorganic nitrogen after rewetting, as observed in both laboratory and field studies (Birch, 1958, 1960; Cui and Caldwell, 1997). It is commonly attributed to microbial cell lysis, the mineralization of dead microbial biomass, and the decomposition of osmoregulatory compounds released during rewetting (Fierer and Schimel, 2002; Jarvis et al., 2007; Saetre and Stark, 2005; Unger et al., 2010). In the field, this pulse can last several days, with the strongest nitrogen release often occurring within the first few days after rewetting (Cui and Caldwell, 1997). However, after the initial rewetting pulse, inorganic nitrogen pools may increasingly reflect the combined effects of continued mineralization, nitrification, denitrification, microbial immobilization, and transport. Distinguishing these processes from pool-size data alone is challenging, particularly under field conditions where water flow and redox conditions vary strongly with depth and time.

Microbial communities mediate most nitrogen transformation processes in soils, but their responses to drought and rewetting are complex. Soil microbial communities can adapt to repeated drying–rewetting cycles, depending on the frequency, intensity, and duration of such disturbances (Armstrong et al., 2016; Fierer et al., 2003; Veach and Zeglin, 2020). Floodplain soils may therefore show contrasting responses: microbial activity may respond rapidly to rewetting, whereas community

composition may remain comparatively stable over short time scales because of spatial heterogeneity, dormancy, or prior exposure to fluctuating environmental conditions (Moche et al., 2015; Rinklebe et al., 2006). Combining microbial community analyses with extracellular enzyme activities can therefore help distinguish whether drought–rewetting primarily affects microbial activity or also leads to detectable shifts in community composition.

Despite extensive knowledge on preferential flow, the Birch effect, redox-dependent nitrogen transformations, and microbial responses to wetting and drying, these processes are rarely investigated together under realistic field conditions. In particular, it remains difficult to determine how heavy rainfall after summer drought simultaneously affects (i) the depth distribution of newly infiltrated water, (ii) the redistribution of nitrate and ammonium, (iii) the development of redox conditions along the soil profile, and (iv) microbial community composition and activity. This integrated perspective is needed because drought-induced preferential flow may rapidly transport nitrate beyond the biologically active topsoil, while subsequent soil wetting may alter redox conditions and microbial activity in ways that affect inorganic nitrogen pools over the following days. The objective of this study was therefore to assess how a simulated heavy rainfall event after summer drought affects water infiltration, inorganic nitrogen redistribution, redox dynamics, and microbial responses in a fine-textured floodplain soil~~, (ii) to examine the temporal transition from pulse-driven nitrogen cycling (the Birch effect) upon soil rewetting towards redox-driven nitrogen turnover processes, and (iii) to assess the impact of drying and rewetting on soil microbial community structure and activity.~~. Specifically, we aimed to (i) quantify the depth distribution of infiltrating water after heavy rainfall using D^2H_2O-~~labelled~~labeled irrigation water, (ii) assess whether nitrate and ammonium differ in their vertical redistribution after rewetting, (iii) evaluate how in situ redox potentials develop during subsequent moderate irrigation and how these dynamics relate to inorganic nitrogen pools, and (iv) determine whether microbial community composition and extracellular enzyme activities respond to rewetting over a 14-day period. To this end, we conducted a field experiment ~~simulating a one-hour heavy rain event followed by recurrent moderate daily rainfall for 14 days on~~ on a Gleysol ~~that exhibited~~with pronounced drought-induced shrinkage cracks~~ after summer drought. The water of the~~. A one-hour simulated heavy rainfall event with D^2H_2O-~~labelled~~labeled water was ~~spiked with deuterated water as a conservative hydrological tracer, that allowed us to quantify water infiltration depth and distribution.~~followed by recurrent moderate irrigation with non-~~labelled~~labeled water. We monitored depth-resolved in situ redox potentials ~~using permanently installed sensors and took~~, collected soil cores to 50 cm depth from irrigated and dry control plots on day 0, ~~i.e., two hours after the heavy rainfall simulation, on~~ day 6/8, and ~~on~~ day 14~~. The soil samples were analyzed for vertical changes in~~, and ~~analysed~~analyzed soil water content, ~~in isotopic~~δ^2H signatures ~~(δ^2H)~~ of ~~the~~ pore water, ~~in~~ extractable ammonium and nitrate ~~concentrations, in~~, total ~~(~~and active microbial community composition based on DNA ~~level)~~ and ~~active (~~RNA ~~level) microbial community composition, as well as in~~, and extracellular enzyme activities.

2 Materials and Methods

2.1 Study site

The study site is located in the Ammer valley floodplain, ~~approx.~~approximately 7 km ~~West~~west of Tübingen ~~in SW~~, southwestern Germany (48.521266° N, 8.972687° E, 394 m a.s.l.). The Ammer catchment ~~of river Ammer~~ is situated in the South German Escarpment ~~in the~~within geological units of the Middle and Upper Triassic. The ~~west~~western part of the catchment lies within the Muschelkalk unit, whereas the eastern part lies within Keuper units, which ~~mostly~~mainly consist of terrestrial sediments~~,~~ such as ~~sand-, mud- or~~ sandstones, mudstones, and dolostones ~~(Geyer et al., 2011; Grathwohl et al., 2013; Martin et al., 2020; Schwientek et al., 2013).~~ (Geyer et al., 2011; Grathwohl et al., 2013; Martin et al., 2020; Schwientek et al., 2013). The floodplain ~~with~~containing the study site ~~lies~~is located in the eastern part of the catchment and is ~~defined~~bordered by Keuper hills ~~at its southern~~to the south

and ~~northern rim~~north. The hydrostratigraphy ~~within~~of the floodplain comprises, from bottom to top~~:~~, Keuper rocks as basement, an aquifer mainly ~~made~~composed of gravel and clay (gravel aquifer), a regional aquitard (lower clay aquitard), a confined aquifer ~~made~~composed of ~~calciferous~~calcareous tufa sediments (tufa aquifer~~)~~), and ~~another~~an upper regional aquitard (upper clay aquitard) ~~(Martin et al., 2020).~~(Martin et al., 2020). The ~~upper clay aquitard comprises the~~ investigated soil~~. On~~ developed within the upper clay aquitard, which is, on average, ~~it is~~ 2 m thick and consists of fine-grained, clay~~-~~-mineral-rich alluvial sediments derived from the surrounding Keuper hills. The ~~bottom half~~lower part of this ~~aquifer~~aquitard is water~~-~~-saturated throughout the year. The soils are ~~characterized~~classified as Gleysols~~, showing the~~ and show typical gleyic properties ~~such as color~~-, including visually distinguishable reduced and oxidized horizons (Appendix A~~) (Martin et al., 2020). In~~; Martin et al., 2020). The 50 cm soil cores collected in this study sampled only the Ah and Go horizons. Although the site is geomorphologically part of the Ammer floodplain, the Ammer currently flows in a regulated riverbed. Regular overbank flooding of the investigated area is therefore unlikely under present ~~study the cores of 50 cm depth only sampled the Ah and the Go horizon~~conditions. This information is relevant for interpreting microbial responses to drying–rewetting and flooding-related redox fluctuations.

The soil ~~has an~~ organic matter content ~~(~~, quantified as total organic carbon (TOC~~), for~~; methodological details ~~see~~in Appendix B~~) of~~), was 2–2.5 wt% in the upper 15 cm and ~~of~~ approximately 1 wt% ~~at~~between 15 ~~to~~and 50 cm depth ~~(Appendix B). It has a uniform soil~~. Soil texture ~~of~~ was relatively uniform within the upper 50 cm, with 11 ± 4 wt% ~~of~~ sand, 56 ± 6 wt% ~~of~~ silt, and 32 ± 4 wt% ~~of~~ clay ~~within the upper 50 cm~~ (Appendix C~~:~~; determined ~~after~~according to DIN EN ISO 17892-4). ~~The soil~~Soil pH ~~varied between~~ ranged from 7.0 ~~and~~to 7.3 and was determined on six samples from irrigated plots, with two samples each from ~~soil depths of~~ 0–10 ~~cm~~, 20–30 ~~cm~~, and 40–50 cm depth, after stirring the ~~sample~~soil in a 1 : 1 (v : w) ~~mix~~mixture with deionized water for 30 min.

The experiment was conducted on ~~a plot of~~ arable land after the harvest of summer barley ~~harvest~~ and after a prolonged summer dry period ~~during summer (see Section Meteorological Conditions~~(see Sect. 2.2 for ~~more~~meteorological details ~~below~~). Information ~~about the~~on previous land use ~~of the plot~~ was provided by ~~personal communication with~~ the farmer~~:~~. During winter 2018/~~19~~2019, before ~~cropping~~the cultivation of summer barley, a catch crop ~~(~~consisting of radish and mustard~~)~~ was planted and ~~in February 2019 this green manure was~~ incorporated into the soil with a cultivator~~.~~ in February 2019. The plot was fertilized with horse manure in winter 2018/~~19~~2019 and with calcium ammonium nitrate fertilizer (27 % N) in spring 2019. During barley cultivation ~~of summer barley~~, the herbicide Ariane-C ~~(active ingredients:~~was applied, containing 100 g L^{-1} ~~Fluroxypyr~~$^{-1}$ fluroxypyr (as ~~Methylheptylester~~methylheptyl ester, 144 g L^{-1}~~),~~$^{-1}$), 80 g L^{-1} ~~Clopyralid +~~$^{-1}$ clopyralid, and 2.5 g L^{-1} ~~Florasulam) was applied~~$^{-1}$ florasulam.

2.2 Meteorological conditions

The climate ~~in the region of~~at the experimental site is temperate oceanic, with a long-term mean annual precipitation of 718 mm and a mean annual temperature of 9.4 °C ~~(~~for the period 1981–2010~~, (German meteorological service (Dwd), 2024)). From~~ (German Meteorological Service (DWD), 2024). Meteorological data were retrieved from a weather station in Tübingen -Unterjesingen (48.52950° N, 8.98380° E, 439 m a.s.l~~.~~), located close to the ~~actual experimental~~ study site~~) meteorological data were retrieved (Agrarmeteorologie baden-Württemberg, 2021) (~~ (Agrarmeteorologie Baden-Württemberg, 2021; Appendix D). The experiment was conducted from 16 to 30 July 2019. ~~In~~During the two weeks preceding ~~experimental~~the start~~,~~ of the experiment, daily temperatures ~~well above~~exceeded 20 °C ~~dominated~~ on all but two days, and three moderate ~~(according to the classification of the American meteorological society (2012))~~ rainfall events occurred ~~(~~, with 9.1, 5.1, and 33.1 mm precipitation, respectively~~).~~ , according to the classification of the American Meteorological Society (2012).

During the experiment, ~~a~~the minimum night-time temperature ~~of~~was 10.2 °C ~~was reached during night (night~~, with an average ~~17.7°C) and a maximum~~ night-time temperature of ~~36.3~~17.7 °C ~~during~~. The maximum daytime ~~(day~~temperature was 36.3 °C, with an average daytime temperature of 24.5 °C~~). On~~ . Temperatures exceeded 25 °C on 12 days~~, temperatures > 25°C~~ and 30 °C on six ~~of these temperatures > 30°C were measured.~~days. Following the FAO guideline ~~(Allen et al., 1998),~~ (Allen et al., 1998), the reference evapotranspiration ~~ET₀~~(ET_0) for July 2019 was calculated as 4.2 mm day^{-1} ~~(see~~ $^{-1}$ (Appendix E). Because the experimental plots had been harvested before the experiment, ET_0 is used here as a meteorological reference for ~~details on the calculation). From 16 to~~atmospheric evaporative demand rather than as a direct estimate of plot-scale evapotranspiration.

Between 16 and 30 July 2019, two natural rainfall events occurred~~,~~: one on ~~the~~ 21 July from 02:00 to 05:00 ~~am~~local time (2.5 mm~~)~~), and ~~a~~one heavy rainfall event from 26 July ~~08~~at 20:00 ~~pm~~ to 27 July at 05:00 ~~am~~local time (24.7 mm~~) (~~; Appendix D). During both ~~of these~~ events, the dry control plots were covered ~~by~~with plastic ~~foils~~foil. However, during the natural heavy rainfall event ~~of~~from 26 ~~July~~ to 27 July, the plastic foil ~~of~~covering plot D2, where the redox probes were installed, was removed by wind.

2.3 Experimental setup

2.3.1 Plot design

The ~~plot~~experimental design comprised nine plots ~~that were~~ arranged as a Latin ~~Square~~square with three ~~different~~ treatments ~~(Fehler: Verweis nicht gefunden). All plots were of 2.4 m~~ (Fig. 1). Each plot had a lateral length of 2.4 m and was separated from adjacent plots by 50 cm ~~stripes to allow~~ access strips. Within each plot, a ~~sampling area of~~ 2 m ~~x~~× 2 m inner sampling area was defined to ~~exclude~~minimize boundary effects. Three ~~different~~ treatments were ~~realized~~established, but only two are relevant for the present study ~~presented here~~: (i) ~~W plots were artificially~~ irrigated ~~to simulate~~ plots (W), where a heavy rainfall event (HRE) after ~~a dry period,~~ drought was simulated, and (ii) dry control plots (D ~~plots~~), which remained dry ~~and served as controls.~~. The third treatment included ~~the~~glyphosate application ~~of glyphosate~~ before irrigation~~. Results~~; results from these plots are presented ~~in other publications (Schlögl et al., 2022; Wirsching et al., 2022).~~elsewhere (Schlögl et al., 2022; Wirsching et al., 2022).

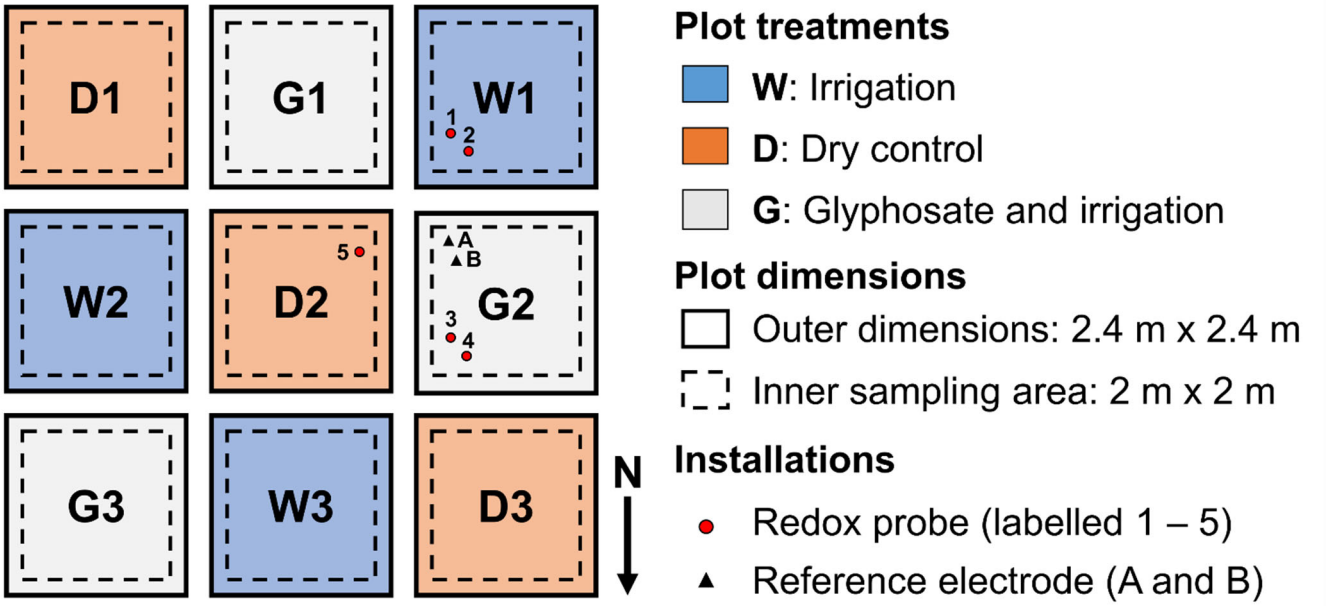


Figure 1: Plot design and treatments in the field experiment. Nine plots of 2.4 m ~~x~~× 2.4 m lateral length were arranged as a Latin ~~Square~~square, and three treatments were ~~realized~~established in ~~triplicates:~~triplicate. A heavy rainfall event was simulated ~~at~~on day 0 ~~and~~, followed by light daily irrigation ~~followed~~ for 14 days on irrigated plots (W plots, blue). Dry control plots (D plots ~~(~~, orange) remained dry ~~and served as control~~. Glyphosate-treated plots~~.~~ (G plots ~~(~~, grey) ~~were treated with~~ received glyphosate before ~~they received~~ the same ~~rainfall~~irrigation treatment as the W plots. ~~An~~The inner sampling area (dashed line) was defined to minimize boundary effects. For ~~the~~ in situ monitoring of redox potentials, redox sensors (red circles) were installed on plots W1, D2, and G2, and two reference electrodes (black triangles A and B, ~~where~~with B ~~served~~serving as ~~control for the~~a system control) were installed on plot G2 ~~approx. in equidistance to~~approximately equidistant from all redox sensors. ~~(~~Figure adapted ~~after *Schlögl et al. (2022).)*~~from Schlögl et al. (2022).

2.3.2 Plot treatment

Irrigation ~~took place~~ was conducted from ~~the~~ 16 to 31 July 2019, with the day of the simulated heavy rainfall event (16 July) defined as day 0 (T0~~) (Fehler: Verweis nicht gefunden).~~; Fig. 2). All plots were covered for one week before the experiment to ~~guarantee~~establish dry initial conditions. The heavy rainfall event ~~(~~, defined as 7.6 to 50 mm ~~per hour by the American meteorological society (2012))~~h^{-1} according to the American Meteorological Society (2012), was simulated by ~~irrigation with~~applying 24.3 mm deionized water ~~for approx.~~over approximately one hour ~~with~~using watering cans. The irrigation water was ~~labelled~~labeled with deuterated water (~~D_2O~~D_2O) as a conservative hydrological tracer. Two ~~liters~~litres of ~~deuterated water~~D_2O (99.9 atom %, Carl Roth, Germany) were mixed with ~~the~~1000 L irrigation water ~~(1000 L) which resulted~~, resulting in an input ~~δ^2H~~δ^2H signature of 12 730 ‰ ~~vs.~~relative to Vienna Standard Mean Ocean Water (VSMOW).

On days 1 to 10 and on day 14, light irrigation with non-~~D_2O labeled~~~~labelled~~labeled water was ~~conducted with an irrigation~~applied at a rate of 5.2 mm day^{-1}. This moderate recurrent irrigation was intended to keep the ~~soils~~soil moist ~~and to force~~, promote the closure of shrinkage cracks ~~to investigate the~~, and allow monitoring of the subsequent development ~~and influence~~ of in situ redox ~~potential on~~potentials, inorganic nitrogen ~~turnover processes~~pools, and ~~on the~~ microbial ~~community~~responses. Daily irrigation was paused from T11 to T13 ~~due to~~because of a natural heavy rainfall event on the evening of T10 and ~~ongoing~~continued natural ~~rain fall~~rainfall on T11 and T12. The ~~D~~dry control plots were covered with greenhouse foil between T10 and T14 to prevent wetting by ~~a~~ natural ~~heavy rainfall on the evening of T10 and the following three days~~rainfall. During the natural heavy rainfall event from 26 to 27 July, the plastic foil covering plot D2, where the redox probes were installed, was removed by wind.

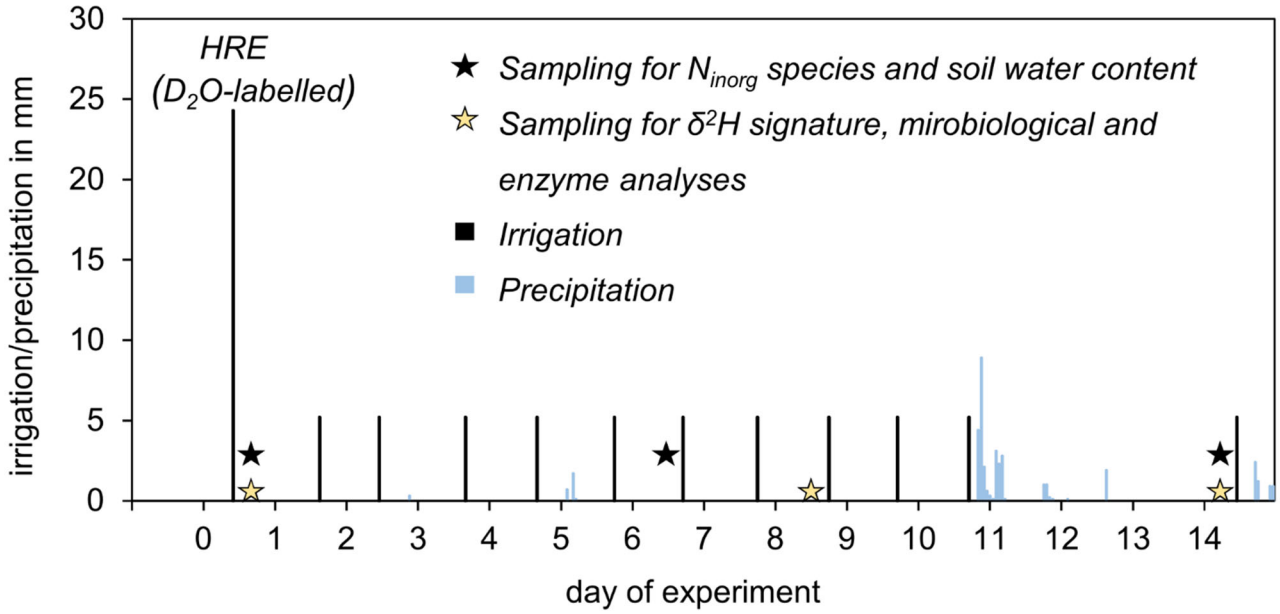


Figure 2: Irrigation and sampling scheme. Irrigation (black bars~~,~~; bar length indicates intensity) included a simulated heavy rainfall event (HRE) with ~~D2O-labeled~~D2O ~~-labelled~~labeled water on day 0, followed by light daily irrigation ~~on~~ with non-~~labelled~~labeled water on W plots. Natural precipitation is indicated by light–blue bars~~, which~~ and was excluded from D plots but not from W plots. Sampling for inorganic nitrogen species (~~Ninorg~~N inorg) and soil water content took place on days 0, 6, and 14 (black stars~~), samples~~). Samples for analyses of ~~δ2H signature~~δ2H signatures, microbial communities, and ~~enzymes~~enzyme activities were ~~retrieved~~collected on days 0, 8, and 14 (golden stars). ~~(~~Figure adapted ~~after *Schlögl et al. (2022).)*~~from Schlögl et al. (2022).

2.3.3 Sampling

~~Sampling~~ Soil sampling was ~~done~~performed with a stainless-steel soil corer (Humax, Hasli-Rüegsau, Switzerland). ~~The soil~~Soil cores were ~~retrieved within~~ collected in PVC liners of 50 cm length and 3.5 cm diameter and were immediately ~~put~~placed on dry ice. In the ~~lab, they~~laboratory, cores were stored at ~~-~~–80 °C ~~(~~for microbiological analyses, enzyme analyses, ~~δ2H~~and δ2H analyses~~)~~, and at ~~-~~–21 °C ~~(~~for inorganic nitrogen ~~species) until further analysis. The~~ analyses. Sampling holes in the field were filled with bentonite.

~~The sampling scheme comprised~~ Two sampling schemes were used: one for ~~(i)~~ inorganic nitrogen species and soil water content, and ~~(ii)~~one for soil pore–water ~~δ2H~~δ2H, microbial community structure, and ~~soil enzymes (Fehler: Verweis nicht gefunden).~~extracellular enzyme activities (Fig. 2). For ~~the~~soil-water δ2H analysis ~~of soil water δ2H~~, cores were ~~taken~~collected from W plots along shrinkage cracks. Additional ~~samples were taken~~cores from D plots were collected to determine the natural ~~δ2H~~δ2H background. Samples for inorganic nitrogen species, soil water content, and microbiological analyses were ~~taken~~also collected from W and D plots along shrinkage cracks. The initial shrinkage cracks were marked before the first irrigation so that their locations remained identifiable during later ~~stages of~~sampling.

Exact sampling positions within each plot were not recorded. However, all samples were taken from within the inner sampling area and at least 20 cm away from plot borders to minimize boundary effects. Later samples were collected at least 10 cm away from previous sampling holes. Because the ~~experiment, their course~~holes were filled with bentonite immediately after coring, direct resampling of disturbed locations was ~~still recognizable.~~avoided. Sample codes ~~in the following text~~ are defined as follows: treatment ~~of the respective plot~~ (dry ~~(~~control, D~~),~~; irrigated ~~(~~, W~~))~~), followed by the ~~respective experimental~~ plot replicate number (1, 2, or 3) ~~as well as~~and the sampling time point T ~~+ number, where~~plus the ~~number expresses the~~experimental day. For example, W1T8 refers to ~~the~~ irrigated plot W1 sampled ~~at~~on day 8, ~~while~~whereas WT8 refers collectively to all three ~~replicate W~~irrigated plots sampled on day 8.

2.3.4 In situ monitoring of redox potentials

~~To evaluate the redox potential as a controlling factor of the microbial turnover of the two inorganic nitrogen species, nitrate and ammonium, in~~ In situ soil redox potentials were ~~measured on a plot irrigated with water (plot~~ monitored to assess temporal and depth-resolved changes in soil redox conditions after irrigation. Measurements were performed on one irrigated plot (W1) with two independent redox sensors (~~sensor~~sensors 1 and 2) and on ~~a~~one dry control plot (~~plot~~ D2) with one redox sensor (sensor 5~~) (Fehler: Verweis nicht gefunden).~~; Fig. 1). Thus, redox measurements provide high-resolution temporal information but were spatially limited to one irrigated and one dry control plot. The multilevel redox sensors (PaleoTerra, Oijen, ~~The~~the Netherlands) ~~were made~~consisted of ~~fiberglass~~fibreglass and epoxy tubes ~~and were~~ with a total length of 1.20 m ~~length~~. Each sensor ~~had~~contained 10 platinum ~~(Pt)~~ electrodes. For ~~the~~ installation ~~of the sensors, we first drilled a~~, vertical ~~hole~~ holes were drilled into the soil ~~that was~~ with a diameter 2 mm smaller ~~in diameter~~ than that of the sensors~~, so that after sensor installation, the~~ to ensure contact between the electrodes and the surrounding soil ~~was given. Then the sensors~~after installation. Sensors were installed ~~in a way~~such that the ~~first~~uppermost electrode was ~~placed~~positioned 5 cm below ground level (bgl~~) and the further~~), with additional electrodes placed at 10 cm intervals ~~bgl.~~below the surface. Two Ag/AgCl reference electrodes (A and B~~) (~~; saturated KCl ~~sat.; E^0~~; E_σ^0~~ = 0.199 V) were installed on plot G2 ~~(Fehler: Verweis nicht gefunden).~~, approximately equidistant from the redox sensors (Fig. 1). One ~~of them served as the~~ reference electrode was used for the measurements, and the ~~other one~~second served as a ~~control for the~~ system control. The redox sensors and reference electrodes were installed on 15 July 2019~~.~~, one day before the start of the irrigation experiment. Measured redox potentials (E_{meas}) are reported ~~vs.~~relative to the standard hydrogen electrode (SHE; ~~E^0~~E_σ^0 = 0 V~~,~~ by definition) as $E_H = E_{meas} + E_{KCl,sat}$. Measurement precision was ± 10 mV. ~~The sensors~~Sensors and ~~the~~ reference electrodes were connected to a data logger (Campbell ~~Scientific~~Scientific, Logan, Utah, ~~US)~~USA), which ~~stored the~~recorded redox potentials at 30 ~~minute~~ min intervals throughout the experiment. ~~The characterization of the in~~In situ soil redox conditions ~~will be based on the following categorization (Mansfeldt, 2003) of~~ were classified according to Mansfeldt (2003) for E_H values at circumneutral pH as follows: oxidizing (> +400 mV vs. SHE), weakly reducing (+400 to +200 mV), moderately reducing (+200 to ~~–~~–100 mV~~)~~), and strongly reducing (< ~~–~~–100 mV).

2.3.5 Soil water content

~~For the assessment of gravimetric~~Gravimetric soil water content ~~on~~was determined for 50 cm soil cores from irrigated (W) and dry control (D) plots~~, the 50 cm cores~~. Cores were ~~cut~~divided into 5 cm increments ~~of 5 cm~~ for 0–10 cm depth and into 10 cm increments ~~of 10 cm~~ for 10–50 cm depth. From ~~these increments, triplicates of approx.~~each increment, three aliquots of approximately 1.5 g ~~of~~ field ~~wet~~ moist soil ~~(scale precision 0.001 g)~~ were weighed ~~(small pebbles were rejected)~~ before and after freeze ~~drying. The gravimetric~~ drying. Small pebbles were removed before weighing. Gravimetric water content (g g^{-1}~~)~~$^{-1}$) was calculated as ~~the ratio of~~ water loss relative to dry ~~weight. The~~ soil mass. Soil water content of ~~the~~ D plots on day 0 was used as the reference condition and is hereafter referred to as ~~"~~the initial soil water content~~"~~.

2.4 Chemical and isotopic analyses

2.4.1 δ^2H signature of soil water

The ~~δ^2H~~δ^2H signature of ~~the~~ soil pore water was determined by ~~H_2O~~H_2O(liquid~~) H_2O(vapor)~~ H_2O(~~vapour~~vapor) equilibration ~~and~~followed by cavity ring-down laser spectroscopy (Picarro L2120-i and L2130-i~~) (Wassenaar et al., 2008). To this end, frozen~~; Wassenaar et al., 2008). Frozen core samples ~~(cores~~from WT0~~/8/14~~, WT8, WT14, and DT0~~)~~ were sliced ~~in~~into 10 cm segments ~~and aliquots~~. Aliquots of 66 ~~to~~ –170 g ~~of those segments~~ from each segment were ~~doublebagged~~double-bagged in 1 L Ziploc freezer bags and stored at 4 °C. Before analysis, the bags were filled with laboratory dry air and ~~the bags were~~ stored for ~~3 more~~an additional three days to ~~let the~~allow equilibration between pore water ~~equilibrate with the~~ and headspace water ~~vapor~~vapour~~vapor~~. Each analysis lasted up to 30 ~~minutes~~min, until the signal ~~plateaued, that is,~~reached a stable

~~conditions~~plateau within the expected measurement accuracy ~~were reached (i.e., ~~, defined as a standard deviation < 1.0 ‰ for ~~δ^2H~~δ^2H of ~~the~~ water ~~vapor).~~ ~~vapour~~vapor. The average signal over the ~~last~~final minute of ~~the~~ analysis was recorded. After every third sample, an internal standard ~~(~~consisting of water ~~of~~with known isotopic composition in a freezer bag~~)~~ was measured for calibration. ~~The isotopic~~Isotopic signatures are reported ~~as isotope ratios~~ relative to ~~the international standard (~~Vienna Standard Mean Ocean Water~~, VSMOV~~ (VSMOW) in delta notation ~~in ‰ (δ‰ = ((R_{sample} − $R_{standard}$)/$R_{standard}$)*1000),~~as δ‰ = ((R_{sample} − $R_{standard}$) / $R_{standard}$) × 1000, where R is the $^2H/^1H$ isotope ratio $^2H/^1H$ of the sample ~~and the~~or standard, respectively. For ~~the~~ determination of ~~δ^2H~~the natural δ^2H background ~~values on cores from~~ in DT0 cores, the ~~upper-most~~uppermost segment was ~~ignored~~excluded to avoid ~~corruption~~potential contamination by wind drift or water ~~vapor~~~~vapour~~vapor from irrigation. ~~Additionally, the gravimetric~~Gravimetric water content of each ~~analyzed~~~~analysed~~analyzed segment was additionally determined ~~by~~from the weight difference before and after drying at 105 °C. These values were used for isotope mass-balance calculations.

2.4.2 Water mass balance

A water mass balance was ~~determined~~calculated to ~~assess~~estimate how much of the total water input from irrigation ~~plus~~and natural precipitation ~~received~~was stored within the sampled 0–50 cm soil profile on days 0, 6, and 14. Total water inputs to W plots were 24.3 mm by day 0, ~~6 and 14 (24.3 mm,~~ 60.0 mm by day 6, and 115.0 mm~~, respectively) on W plots reached the different depth segments of the profile. It was assumed that irrigation only led to a water storage change and that hardly any leaching below 50 cm occurred.~~ by day 14. The measured gravimetric soil water contents from WT0~~/6/14~~, WT6, WT14, and DT0 were converted to volumetric water contents using known bulk densities of ~~individual~~the corresponding depth segments. The change in water storage within each depth ~~segments. With these volumetric water contents, the amount of water volume change~~segment was calculated ~~and~~relative to the ~~increase of~~initial soil water content~~, i.e.,~~ of the dry control plots on day 0 and expressed as water volume per ~~m² on irrigated plots, at each day was assessed by comparison with dry plots on day 0.~~square metre. The resulting water mass balance represents apparent water recovery within the sampled 0–50 cm soil profile. It does not constitute a closed hydrological balance, because water loss by evaporation and drainage below 50 cm depth could not be quantified directly from soil water content measurements alone. Potential losses below the sampled depth were therefore evaluated indirectly using the δ^2H isotope mass balance of the ~~labelled~~labeled heavy-rainfall water.

2.4.3 Isotope mass balance

The irrigation water ~~of~~applied during the simulated heavy rainfall event on day 0~~,~~ (Irr_{HRE}) was ~~labeled~~~~labelled~~labeled with D_2O. A two-component ~~(i.e., isotope mass balance)~~ mixing ~~approach~~model was used to calculate the fraction of Irr_{HRE} in ~~every i-th~~each depth segment ($f_{IW,zi}$):

$$f_{IW,z_i} = \frac{\delta^2H_{z_i} - \delta^2H_0}{\delta^2H_{IW} - \delta^2H_0}$$

where δ^2H_{zi} is the measured isotope ratio in the i-th depth segment, ~~δ^2H_{IW}~~δ^2H_{IW} is the isotope ratio of the simulated heavy-rainfall ~~event~~ irrigation water on day 0 (~~i.e., 12-730‰)~~ ‰), and ~~δ^2H_0~~δ^2H_0 is the average natural background ~~average δ^2H~~δ^2H of ~~the~~ pore water before irrigation ~~(i.e., (−47.6‰). For the calculation of~~ -‰). To calculate the amount of ~~Irr_{HRE}~~Irr_{HRE} in each depth segment, the volumetric water content calculated as described in ~~Section~~Sect. 2.4.2 was multiplied by the fraction of irrigation water ~~f_{IW}~~$f_{IW,zi}$.

2.4.4 Extraction and analysis of inorganic nitrogen

~~Changes in the content of~~Extractable inorganic nitrogen ~~compounds~~ was ~~analysed~~analyzed to assess changes in nitrate and ammonium ~~allow to follow redox transformations induced by the~~pools after the simulated heavy rainfall event~~.~~ and during subsequent irrigation. Inorganic nitrogen was extracted from ~~approx.~~approximately 1.2 g ~~of~~ frozen soil aliquots with 12 mL 2 M KCl (p.a., Honeywell, Germany) prepared in ultrapure water (GenPure Pro UV-TOC, Thermo Fisher Scientific, Germany). Samples were shaken for 30 ~~minutes~~min on a horizontal shaker (IKA, Germany) ~~with~~at 160 motions ~~per minute (mpm)~~min^{-1} and then centrifuged at room temperature for 15 min at ~~5 000 x~~5000 × g (centrifuge 5430 R, Eppendorf, Germany~~) and~~). Extracts were filtered ~~(~~through 0.2 µm~~,~~ regenerated cellulose~~, filters (~~Sartorius, Germany~~). The extracts were~~), stored at 4 °C ~~until analysis,~~ and ~~were analyzed~~~~analysed~~analyzed within a maximum of ~~2~~two days.

Ammonium and nitrate concentrations were ~~analyzed in these extracts~~determined by continuous flow analysis (CFA) using an AA3 HR AutoAnalyzer System ~~from (~~Seal Analytical~~(~~, Germany). All chemicals ~~used~~ were ~~purchased~~obtained from Sigma~~-~~Aldrich, Germany, and were of ACS grade. Standard ~~curve range was~~curves ranged from 0 to 7.5 mg N L^{-1}~~–1~~ for both analytes~~, giving a~~ and showed high linearity (R^2 ~~between~~= 0.999~~–and–~~1.000). Nitrate ~~determination followed the~~ was determined according to ISO~~-~~13395~~ standard methodology~~, where nitrate is reduced to nitrite by hydrazine~~, which~~ and then reacts with sulfanilamide and NEDD ~~forming~~to form a pink complex~~, which is~~ measured at 550 nm. ~~Potentially~~Nitrite present ~~nitrite~~ in the original sample ~~is~~was determined independently without hydrazine addition and subtracted from nitrate ~~concentration.~~concentrations. Ammonium was determined according to ~~the~~ ISO~~-~~11732~~ standard methodology,~~ where ~~it~~ammonium reacts with salicylate and dichloroisocyanuric acid to form a blue complex ~~which is~~ measured at 660~~-~~ nm. To account for ~~signal shifts due to the sample~~potential matrix ~~(2~~ effects caused by 2 M~~-~~KCl~~),~~, standards for both nitrogen species were also prepared in 2 M KCl ~~for both nitrogen forms.~~.

2.4.5 Nitrate and ammonium mass balance

~~The measured~~Measured nitrate and ammonium concentrations (mg N L^{-1}~~)~~~~–1~~) were corrected for baseline and blank values, and the ~~mass~~masses of nitrate and ammonium in the extraction solution ~~was~~were calculated. The original ~~weight~~mass of the frozen soil sample was corrected to dry ~~weight by the~~ mass using gravimetric water content ~~and the~~. The mass of ammonium-N and nitrate-N per gram ~~of~~ dry soil was then calculated. ~~Including~~Using bulk density ~~of the soil~~ and the ~~sample~~ volume ~~at different depths~~ of ~~the~~each soil core~~, the mass of~~ segment, ammonium-N and nitrate-N ~~at~~ masses were calculated for each depth interval and for the ~~whole~~ entire 0–50 cm soil core ~~was assessed.~~

2.5 Microbiological Analyses

2.5.1 Molecular Analysis

For molecular analysis of bacteria and archaea, soil cores were ~~stored~~placed on dry ice immediately after sampling~~. Soil cores were~~ and stored at −80 °C in the ~~lab at –80°C~~laboratory until analysis. ~~The frozen~~Frozen cores were cut into depth segments ~~ranging from soil depth~~of 0–10 ~~cm~~, 20–30 ~~cm,~~ and 40–50 cm using ~~a~~an electric saw sterilized ~~(~~with 2 % sodium hypochlorite solution~~) electric saw. For nucleic acid extraction representative~~. Representative subsamples ~~(~~of 10–15 g~~) of the~~ soil ~~samples~~ were ~~defrosted~~thawed at room temperature~~,~~ and homogenized with a sterile spatula~~, and finally duplicate~~. Duplicate aliquots of 400 mg ~~of~~from each subsample were used for DNA extraction.

DNA ~~extraction~~ was ~~conducted with~~extracted using the DNeasy PowerSoil Kit (Qiagen, Hilden, Germany) according to the manufacturer's protocol. RNA was extracted using ~~the modification of a~~a modified commercial DNA extraction ~~kit~~protocol according to ~~Tournier et al. (2015)~~Tournier et al. (2015), combining the FastDNA SPIN™ ~~kit~~Kit for ~~soil~~Soil (MP Biomedicals) ~~and~~with the RNaid® Kit (MP Biomedicals, LLC, ~~Illkrich~~Illkirch, France). Instead of the standard ~~weight~~sample mass of 0.25

g, 0.5 g soil was used to increase ~~the mass of~~ RNA yield. RNA was purified ~~with~~using the RNeasy Micro Kit (Qiagen). Residual DNA was removed with ~~DNase~~DNase I, and ~~the~~ RNA was reverse-transcribed to cDNA using the RevertAid RT Reverse Transcription Kit (Thermo Scientific) with ~~a~~ random hexamer ~~primer~~primers. A primer combination of 515F (5′-GTGYCAGCMGCCGCGGTAA-3′) and 806R (5′-GGACTACNVGGGTWTCTAAT-3′), ~~annealing to~~targeting the V4 region of the 16S rRNA gene, was used for ~~gene~~ amplification~~,~~ following the PCR protocol ~~as~~ described by ~~Pjevac et al. (2017).~~Pjevac et al. (2017). Sequencing was performed on ~~a~~an Illumina MiSeq platform (Illumina, San Diego, CA, USA~~),~~) using ~~a~~ v3~~, 600 cycle~~ chemistry with 600 cycles (2 × 300 ~~b~~bp paired-end ~~sequences~~reads) in two separate runs.

Raw reads were processed in R ~~(~~version 4.1.1~~,) with~~ using DADA2 ~~(v.~~version 1.20.0~~),~~ as outlined ~~in Callahan et al. (2017).~~by Callahan et al. (2017). Amplicon ~~Sequence Variants~~sequence variants (ASVs) were inferred across all samples in pooled mode ~~(details~~. Details on sequence trimming~~,~~ and quality filtering ~~is outlined in Pjevac et al. (2017)).~~are provided in Pjevac et al. (2017). ASV sequences were ~~subsequently~~ aligned and classified using SINA version 1.7.2 and the SILVA ~~database~~ SSU Ref NR 99 database release 138.1 ~~using~~with default parameters. ASVs classified as ~~archaea,~~ eukaryotes, mitochondria, or chloroplasts, as well as ASVs not classified at ~~the~~ domain level, were removed before downstream analysis. ASVs classified as archaea were also removed from the dataset ~~prior to~~before downstream analysis; the resulting dataset therefore represents bacterial 16S rRNA gene and transcript diversity. Statistical ~~data analysis was~~analyses were performed ~~with~~in R, and plots were created using ~~the package~~ ggplot2. Alpha and beta diversity indices were calculated ~~(vegan)~~ and compared using vegan. Non-metric multidimensional scaling (NMDS) ~~analysis of Aitchinson~~based on Aitchison distances was used for ordination.

2.5.2 Extracellular Enzyme Activities

Potential activities of three ~~soil~~ hydrolytic soil enzymes, ~~i.e.,~~ β-glucosidase (BG), N-acetylglucosaminidase (NAG; exochitinase~~)),~~ and acid phosphatase (AP~~)),~~ were measured fluorometrically ~~with~~using artificial substrates ~~(Tian et al., 2023).~~(Tian et al., 2023). The following 4-methylumbelliferyl (MUF~~))~~-based substrates were used ~~to measure the enzyme activities~~: MUF-β-D-glucopyranoside for BG, MUF-N-acetyl-β-D-glucosaminide for NAG, and MUF-phosphate for AP. Soil slurries ~~(1:100 (w:v))~~ were prepared in 50 mM sodium acetate buffer (pH 5) at a soil-to-buffer ratio of 1 : 100 (w : v) and dispersed by ultrasonication ~~(~~with an energy input ~~–~~of approximately 350 J~~).~~. Substrates were added to soil slurries in black microplates in five analytical replicates and incubated in the dark for 180 min, with repeated measurements of sample fluorescence. Microplates were read ~~by~~using a TECAN Infinite® M200 spectrophotometer at an excitation wavelength of 365 nm and an emission wavelength of 450 nm. Sample fluorescence was corrected for quenching, and ~~the~~MUF concentrations ~~of MUF~~ released by enzymatic activity were calibrated ~~by respective~~using standards added to ~~the~~ soil slurries.

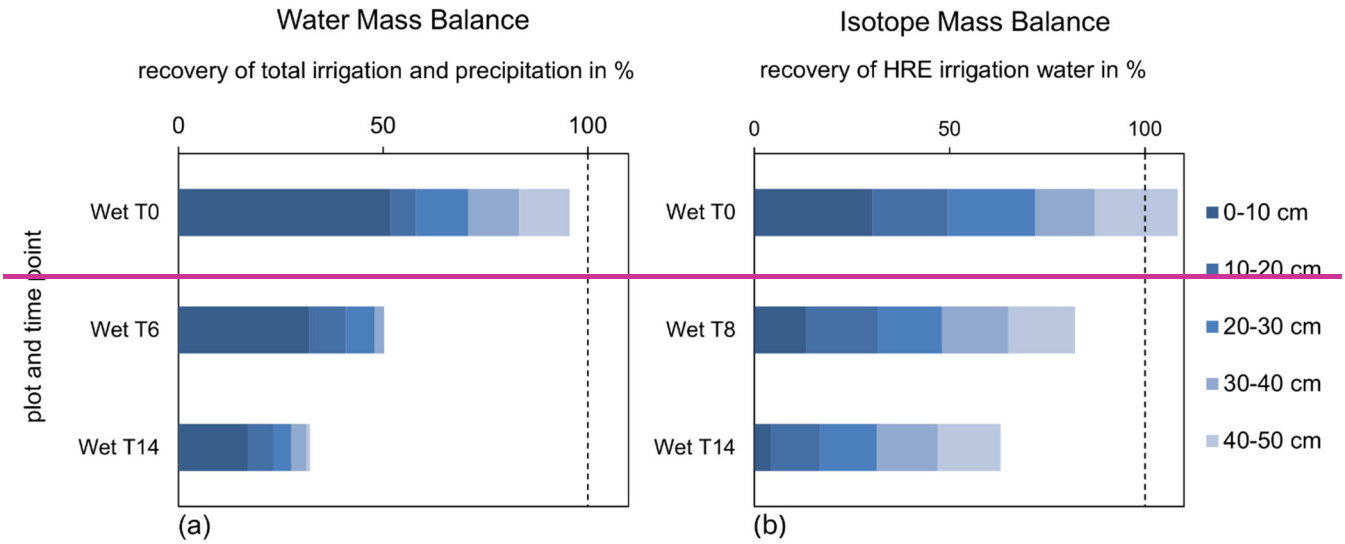
3 Results

3.1 Soil water ~~content~~distribution and in situ redox potentials

~~Water mass balances and ^2H_2O isotope mass balances were calculated for days 0, 6 and 14 and days 0, 8 and 14, respectively (Fehler: Verweis nicht gefundena and b), to measure the infiltration depth of the irrigation water. Mean values were calculated from the triplicate experimental plots for each depth section. For the water mass balance on T14 and the isotope mass balance on T8, mean values were only calculated from two individual plots due to sample loss. The water mass balance (Fehler: Verweis nicht gefundena) included the sum of all irrigation and natural precipitation water during the experiment, Irr_{tot}, whereas the isotope mass balance (Fehler: Verweis nicht gefundenb) only included the recovery of the D_2O labeled heavy rainfall event water, Irr_{HRE}~~The simulated heavy rainfall event rapidly increased soil water storage throughout the sampled 0–

50 cm profile, whereas the recurrent moderate irrigation applied thereafter was retained mainly in the upper soil layers (Fig. 3a). On day 0 (T0), 95.6 % of the applied irrigation water was recovered within the 0–50 cm profile. Apparent recovery of the cumulative water input decreased to 50.3 % at T6 and 32.1 % at T14.

Two-



~~Figure 3: (a). Water mass balance for days 0, 6, and 14 (T0, 6, and 14) in five 10 cm soil depth sections. Recovery of the water is given in relation to the total amount of water that had reached the plots by irrigation and natural rainfall at the respective time point (Irr_{tot}, represented by the 100 % line). (b). Isotope mass balance for days 0, 8 and 14 (T0, T8 and T14) in five 10 cm depth intervals. Recovery of heavy rainfall water is given in relation to the amount of deuterium-labeled irrigation water of the simulated heavy rainfall event (Irr_{HRE}) on T0. The color gradient from dark to light blue indicates the depth from the top (0–10 cm) to the bottom (40–50 cm) of the soil profile.~~

~~The water mass balance was calculated as the percentage of the sum of irrigation and natural precipitation water, Irr_{tot}, recovered in the soil at days 0, 6 and 14 (T0, T6, T14) on irrigated (W) plots (Fehler: Verweis nicht gefundena) after subtracting pre-event water levels from dry plots. Irr_{tot} was 24.3 mm at T0, 60.0 mm at T6, and 115.0 mm at T14 which is represented as the 100 % line in Fehler: Verweis nicht gefundena. The recovery of irrigation plus precipitation water was 95.6 % at T0, 50.3 % at T6, and 32.1 % at T14, and thus steadily decreased during the experiment.~~

~~In the following, the dynamics of irrigation and precipitation water recovery are described as percentages of the amount of recovered water at the time points T0, T6, and T14, respectively. At T0, 2~~ hours after the simulated heavy rainfall event, 54.2- % of the recovered ~~irrigation~~ water was ~~found~~located in the ~~top~~upper 10 cm-, while 19.9 % ~~of the recovered water was found~~occurred at ~~a~~10–30 cm depth ~~of 10–30 cm. A substantial fraction (~~and 25.9 ~~%) however, was~~% had already ~~present in the subsoil (~~reached 30–50 cm depth~~). Also, at~~ (Fig. 3a). At T6 and T14, more than ~~50 %~~half of the recovered ~~irrigation~~ water was ~~found~~again located in the upper 10 cm. ~~At 10–30 cm depth, the percentage of recovered water increased to 31.6 % and 32.6 % at T6 and T14, respectively. However, the absolute amount of Irr_{tot} at 10–30 cm depth decreased compared to T0. At T6 and T14~~In contrast, only small fractions of the recovered water were found at 30–50 cm depth at T6 and T14 (4.7 % and 14.4 %, respectively~~) were found at 30–50 cm depth.~~

~~While the HRE irrigation water at T0, Irr_{HRE}, carried a ^2H label, the irrigation water from the following moderate daily rainfall events was unlabeled.~~). Thus, the ~~recovery of the HRE water could be assessed via an isotope mass balance at T0, T8 and T14 from the soil water content, the fraction of the recovered ^2H label, and the amount of simulated heavy rainfall~~

~~event irrigation water, Irr_{HRE}, (24.3 mm). The recovery was calculated for 10 cm layers of the 50 cm soil cores. The isotope mass balance is presented as the percentage of the simulated heavy rainfall event (24.3 mm) recovered in the soil on days 0, 8, and 14 (T0, T8, T14) on W plots (Fehler: Verweis nicht gefundenb). The Irr_{HRE} was 108 % at T0, 82 % at T8 and 63 % at T14. In the following, the development of the recovery is described as the percentages of the amount of recovered irrigation water from the heavy rainfall event. At T0, the biggest fraction of HRE irrigation water (30 %) was found in the upper 10 cm of the soil. The rest of the irrigation water was fairly evenly distributed throughout the soil profile: each of the 10 cm depth intervals from 10 to 50 cm containing 15–22 % of the recovered irrigation water. On T8 and 14 only 13 % and 4 % of the recovered Irr_{HRE} were found in the top 10 cm, respectively. Also, in the deeper segments the recovery decreased during the experiment but less pronounced compared to the top 10 cm~~initial heavy rainfall event caused rapid deep infiltration, whereas subsequent moderate irrigation contributed mainly to water storage in the topsoil.

The isotope mass balance confirmed rapid redistribution of the D_2O-~~labelled~~labeled heavy-rainfall water throughout the sampled soil profile (Fig. 3b). Recovery of the ~~labelled~~labeled heavy-rainfall water was 108 % at T0, 82 % at T8, and 63 % at T14. Recovery of more than 100 % result from slightly uneven irrigation intensity or confluence of the irrigation water at the shrinkage crack sites where the samples were taken. At T0, 30 % of the recovered ~~labelled~~labeled water was found in the upper 10 cm, while the remaining ~~labelled~~labeled water was distributed relatively evenly across the deeper 10 cm depth intervals, each containing 15–22 % of the recovered label. At T8 and T14, only 13 % and 4 %, respectively, of the recovered ~~labelled~~labeled water remained in the upper 10 cm. The relative decrease in ~~labelled~~labeled water recovery over time was therefore strongest in the topsoil.

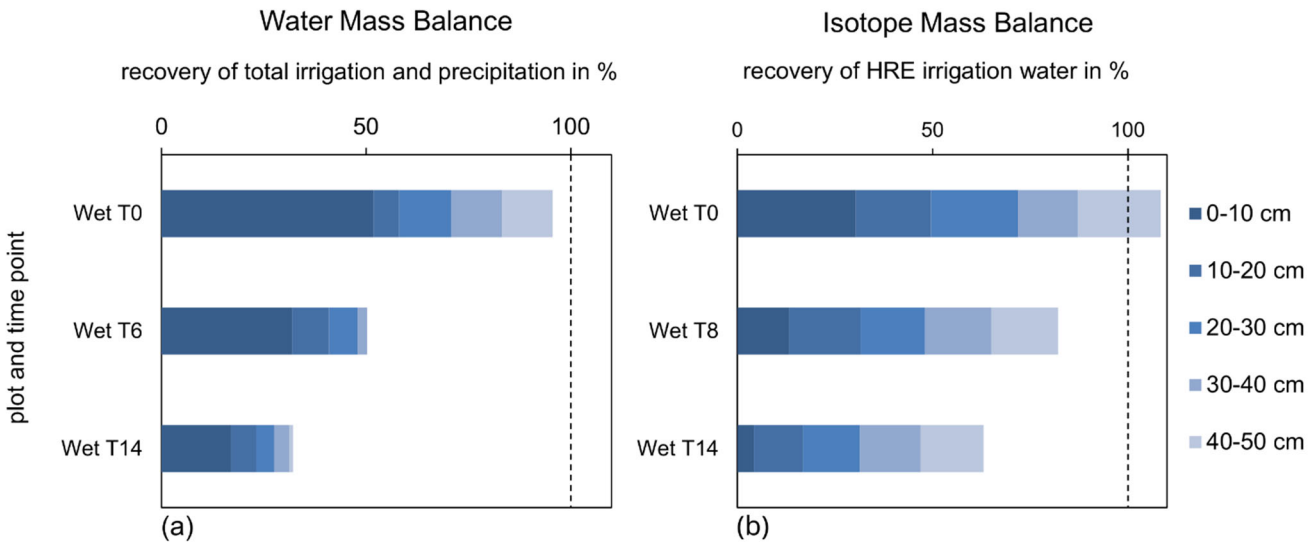


Figure 43: (a). ~~**The in situ redox potentials were measured at different depths from 5 cm below ground to 60 cm below ground (Fehler: Verweis nicht gefunden). In the beginning of the measurements (T0), the in situ redox conditions were oxidizing (> 400 mV vs. SHE) at all depths.**~~ **Water mass balance for days 0, 6, and 14 (T0, T6, and T14) in five 10 cm soil depth intervals. Recovery is shown relative to the total water input from irrigation and natural rainfall received by the plots by each time point (Irr_{tot}; 100 % line). (b) Isotope mass balance for days 0, 8, and 14 (T0, T8, and T14) in five 10 cm soil depth intervals. Recovery is shown relative to the amount of D_2O-~~labelled~~labeled irrigation water applied during the simulated heavy rainfall event on T0 (Irr_{HRE}). The colour gradient from dark to light blue indicates increasing soil depth from 0–10 to 40–50 cm.**

In situ redox potentials responded ~~to the irrigation at all measurement points on W plots. In the topsoil layers (0~~strongly to irrigation and showed pronounced variation with depth and time (Fig. 4). At the start of the experiment, redox conditions were oxidizing throughout the monitored soil profile (> +400 mV vs. SHE). In the irrigated plot, redox potentials declined at all monitored depths after the simulated heavy rainfall event. In the upper soil layers (5–20 cm below ground~~)~~), redox potentials mostly ~~declined~~shifted to reducing conditions within 24~~-~~ h ~~after the simulated heavy rainfall.~~. In the subsoil (30–50~~-~~ cm below

ground), the ~~time for redox potential~~ decline ~~to +200 mV varied between one (sensor 2, 30 cm) and six (sensor 1, 30 cm) days and, thus, on average, was longer than in the top soil but also~~ was slower and more variable~~..~~; the time required to reach +200 mV ranged from one day at 30 cm depth in sensor 2 to six days at 30 cm depth in sensor 1.

~~At 10, 20 and 30 cm soil depth, after the first~~After this initial decline, ~~we observed high temporal and spatial (among sensors) variations in the~~ redox potentials~~, ranging~~ at 10, 20, and 30 cm depth showed strong temporal variation and also differed between the two sensors installed in the irrigated plot. Values fluctuated between oxidizing and moderately reducing conditions~~, whereas at a depth of~~. At 40 ~~to~~ 60 cm ~~below ground~~depth, the ~~decline of~~decrease in ~~situ~~ redox ~~potentials~~potential after ~~the~~ irrigation was more ~~constant.~~

~~Especially~~ gradual and persistent. The strongest short-term fluctuations occurred at 10 cm depth in sensor 1 ~~(plot W1, Fehler: Verweis nicht gefundena) at a depth of 10 cm, the daily irrigation and drying of the soil led to strong diurnal changes of the redox potentials between~~, where redox potentials varied between weakly oxidizing and moderately reducing conditions ~~(+200 mV to -100 mV). Between days 10 and 14,~~during the phase of recurrent irrigation. When daily irrigation ~~of 5.2 mm~~ was interrupted~~,~~ between T10 and T14, redox potentials ~~rose well into~~increased again, reaching weakly reducing ~~or~~to oxidizing conditions even at ~~soil depths of 30 to 50 cm. At the dry plot (plot D2, Fehler: Verweis nicht gefundene and f), the redox potentials remained oxidizing throughout the experiment, except of 10 and 20 cm soil depth at day 10 to 14, when a natural heavy rainfall event hit the experimental plots and removed the protecting foil from plot D2 (but not the other dry treatment plots).~~ 30–50 cm depth.

In the dry control plot, redox potentials remained oxidizing throughout most of the experiment (Fig. 4). The only exception occurred between T10 and T14 at 10 and 20 cm depth, when the plastic foil covering plot D2 was removed by wind during a natural heavy rainfall event.

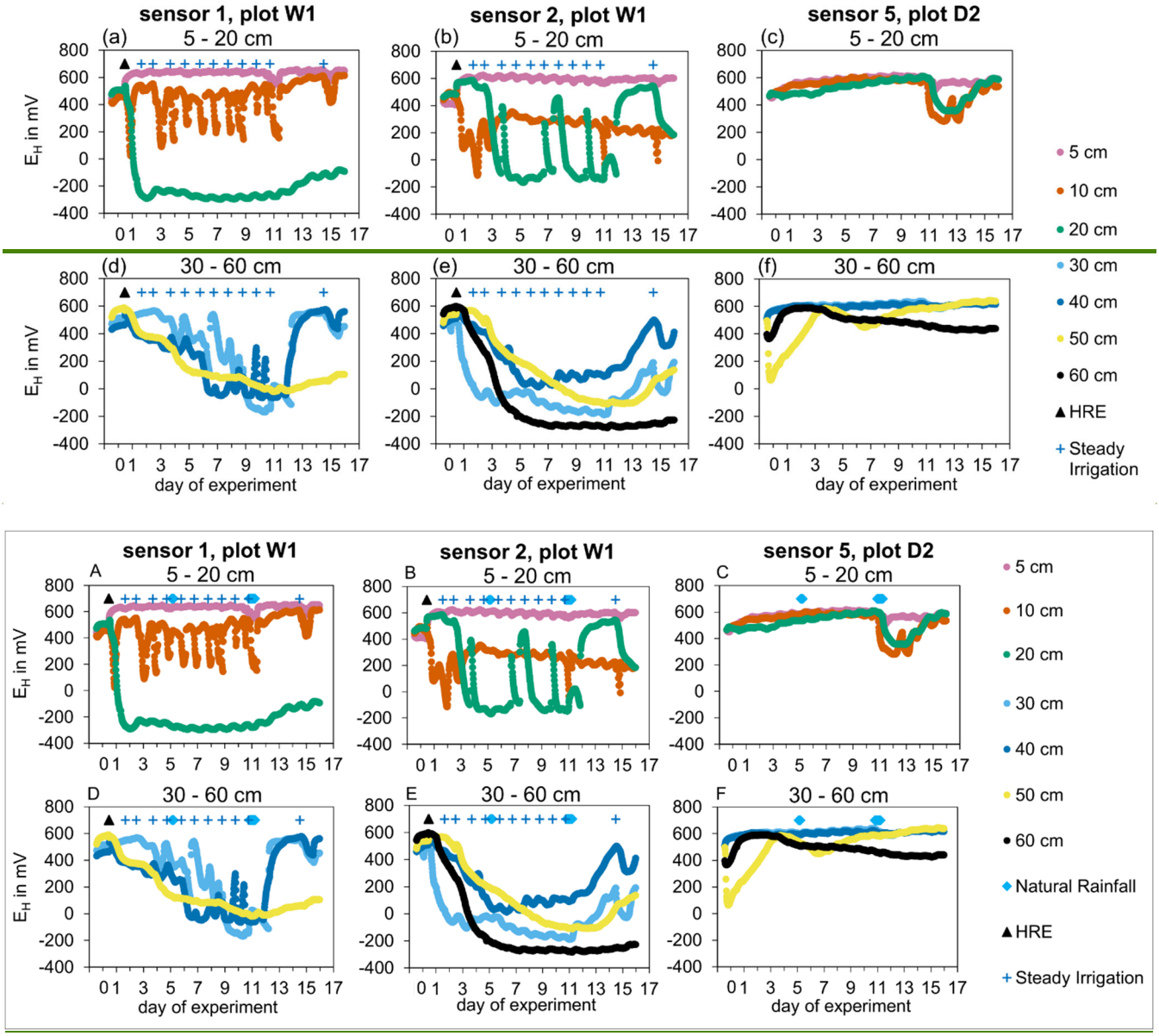


Figure 54: In situ redox potentials (, reported as E_H at pH7 in mV vs. SHE) were, measured on plot W1 (irrigated plot W1 with water, sensor 1 and 2)two sensors and on plot D2 (dry control, plot D2 with one sensor 5). Redox potentials are shown at depths of 5, 10, and 20 cm depth (panels (a) to (c)) and at 30, 40, 50, and 60 cm depth (panels (d) to (f)). The measurements). Measurements started on experiment day T−1 and are presentedshown until T16. For plot W1, the time points of the simulated heavy rainfall event (HRE;; black triangle) and the steadysubsequent light irrigation events (blue crosses) are indicated, and for all plots, the natural heavy rainfall events (blue diamonds) are depicted (panels (a), (b), (d) and (e)).indicated.

3.2 Nitrogen CycleInorganic nitrogen masses

Ammonium The simulated heavy rainfall event affected ammonium and nitrate masses differently (Fig. 5). Ammonium mass balances were calculated to evaluate increased only in the nitrogen solute transport and the turnover of the two inorganic nitrogen species. Dry control plots on day 0 (DT0) represent the initial state of theuppermost soil inorganic nitrogen before irrigation. A comparison of DT0 with irrigated plots on day 0 (WT0), 2 hlayer after the irrigation, therefore, indicates the impact of irrigation on the inorganic nitrogen species distribution rewetting, whereas nitrate mass decreased across the soil upper part of the profile.

shortly after irrigation.

Two hours after the simulated heavy rainfall event, ammonium ~~(Fehler: Verweis nicht gefundena) had~~mass in the 0–5 cm layer nearly doubled ~~in the top horizon (0–5 cm),~~ , increasing from 0.08 ± 0.03 mg N ~~(DT0)~~in dry control plots at T0 to 0.15 ± 0.02 mg N ~~(WT0)~~in irrigated plots at T0 ($p < 0.05$~~). On W plots at 0–5 cm depth,~~; Fig. 5a). In the same layer, ammonium ~~contents~~mass further increased to 0.20 ± 0.01 mg N at T6 ($p = 0.058$ compared with WT0) and 0.3 ± 0.2 mg N at T14 ($p > 0.05$~~).~~ compared with WT0). Below 5 cm ~~soil~~ depth, ~~only minor changes in soil~~ ammonium ~~content occurred~~masses changed only slightly during the experiment~~, the sum of~~. Consequently, total ammonium ~~over~~mass in the ~~entire~~ 0–50 cm ~~soil~~ profile ~~therefore being very~~remained similar ~~at DT0, WT0, WT8 and WT14 (~~in irrigated plots across T0, T6, and T14, ranging between 0.8~~–~~ and 0.9 mg N~~). However, the sum of ammonium in DT14 (1.2 ± 0.3 mg N) was nearly twice as high as in DT0 ($p > 0.05$). From DT0 to DT14, ammonium mass increased at all depths, three-fold at 0–5 cm ($p < 0.05$) and 1.1-fold to 2.2-fold at greater depth (all $p > 0.05$).~~ .

In dry control plots, total ammonium mass increased from 0.8 ± 0.1 mg N at T0 to 1.2 ± 0.3 mg N at T14, although this increase was not statistically significant ($p > 0.05$). The strongest relative increase occurred in the 0–5 cm layer, where ammonium mass increased approximately three-fold ($p < 0.05$). At greater depth, ammonium mass increased by factors of 1.1 to 2.2, but these changes were not significant.

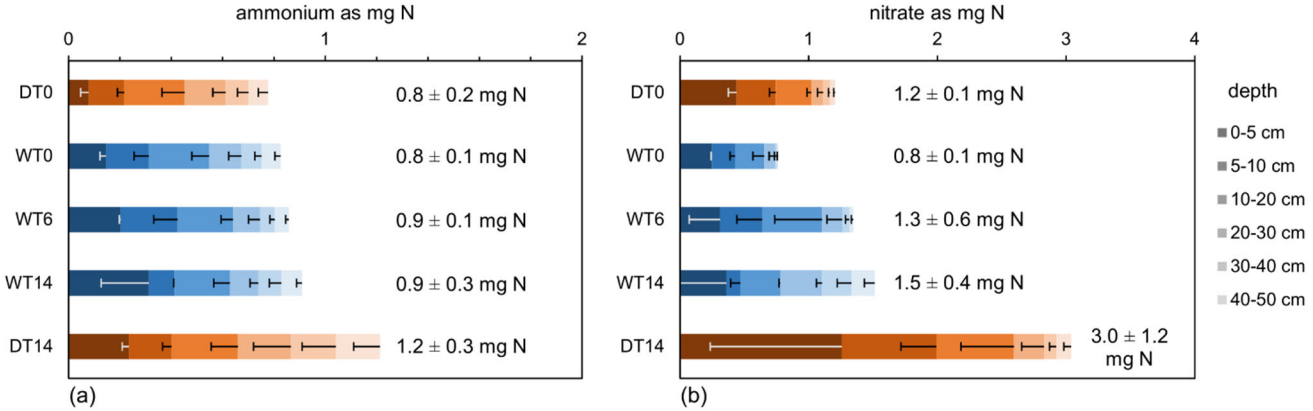


Figure ~~65~~: Mass balance of ammonium (~~panel (~~a~~)~~) and nitrate (~~panel (~~b~~)) (each)~~, expressed as mg N per core segment~~),~~ in ~~cores from~~ dry control plots on ~~day~~days 0 and ~~day~~ 14 (orange bars~~,~~; DT0 and DT14) and ~~on~~in irrigated plots on days 0, 6, and 14 (blue bars~~,~~; WT0, WT6, and WT14). ~~Color~~Colour shading from dark to light ~~symbolizes~~indicates increasing soil depth ~~of the core segments. Displayed are the~~. Bars show means of three ~~experimental triplicates and their~~replicate plots, and error bars indicate standard deviations. ~~The sums of~~Total ammonium and nitrate ~~contents together with their standard errors~~masses in ~~each~~ the 0–50 cm ~~core~~profile are ~~displayed on~~shown to the right of the ~~bars.~~stacked bars, together with standard errors.

Nitrate showed a contrasting pattern. Total nitrate mass in the ~~whole~~0–50 cm profile ~~(Fehler: Verweis nicht gefundenb)~~ decreased by approximately one third ~~shortly~~within two hours after irrigation~~ (~~, from 1.2 ~~±~~ ± 0.1 mg N in ~~DT0 vs.~~dry control plots at T0 to 0.8 ± 0.1 mg N in ~~WT0,~~ irrigated plots at T0 ($p < 0.05$; Fig. 5b). This decrease was ~~mostly caused by a~~driven mainly by losses from the upper soil layers. Nitrate mass decreased by approximately 40 % ~~decrease~~ at both 0–5 ~~cm~~ and 5–10 cm ~~soil~~ depth (both $p < 0.05$) and ~~an~~by 18 % ~~decrease~~ at 10–20 cm depth ($p > 0.05$). ~~From WT0 to WT14, during ongoing moderate daily irrigation (5.2 mm day^{-1}),~~

During the ~~whole profile~~following two weeks, nitrate mass ~~almost~~in irrigated plots increased again. Total nitrate mass nearly doubled from 0.8 ± 0.1 mg N at WT0 to 1.5 ± 0.4 mg N at WT14 ($p < 0.05$). From WT0 to WT6, nitrate mass increased ~~at 0–5 cm, 5–10 cm and 10–~~mainly in the upper 20 cm, while ~~there were no relevant~~ changes below 20 cm ~~depth~~were small. From WT6 to WT14, nitrate ~~increased at~~ mass increased in the 0–5 cm layer and also below 20 cm depth, whereas nitrate masses at 5–10 and 10–20 cm depth decreased; however, these depth-specific changes were not significant.

In dry control plots, total nitrate mass increased from 1.2 ± 0.1 mg N at T0 to 3.0 ± 1.2 mg N at T14, but this increase was not statistically significant ($p > 0.05$). The increase occurred mainly in the upper soil layers, with an approximately three-fold increase at 0–5 cm ~~and below 20 cm and decreased~~ depth ($p > 0.05$), a 2.4-fold increase at 5–10 cm depth ($p < 0.1$), and a 2.2-fold increase at 10–20 cm ~~(all~~ depth ($p > 0.05$).

~~**On D plots, the sum of nitrate mass showed a 2.5-fold increase from T0 (1.2 ± 0.1 mg N) to T14 (3.0 ± 1.2 mg N) ($p > 0.05$) (Fehler: Verweis nicht gefundenb). This strong increase of nitrate was mainly due to a strong increase in the upper soil layers: a nearly 3-fold increase in the top segment (0–5 cm) ($p > 0.05$) and a 2.4- and 2.2-fold increase at 5–10 cm ($p < 0.1$) and 10–20 cm ($p > 0.05$), respectively.**~~

3.3 Microbial community composition and extracellular enzyme activities

~~To assess the effect of a heavy rainfall after a summer drought and the following changes in soil redox potentials on soil microbial community composition and activities, the depth- and time-resolved in situ redox potentials (E_H) were recorded as well as total (on DNA level) and active (on RNA level) soil microbial community composition at depths of 0–10 cm, 20–30 cm and 40–50 cm from dry (D) and wet (W) plots on days 0, 8 and 14.~~

~~The~~ Microbial community composition showed high spatial variability but no clear separation between irrigated and dry control plots over the 14-day experiment. After quality filtering, the 16S rRNA amplicon ~~sequencing resulted in~~ dataset contained a mean ~~number~~ of ~~7 401~~7 401 reads per sample for DNA and ~~6 970~~6 970 reads per sample for RNA. ~~Due to the large range of reads per sample (DNA: min: 3 531; max: 13 706, and RNA: min: 8; max: 18 224), we selected~~Because read numbers varied strongly among RNA samples, only samples with at least 300 reads~~, thereby~~ were retained, reducing the RNA dataset from 54 to 46 samples. ~~These~~The retained samples contained, on average ~~1 334 different Amplicon Sequence Variants,~~ 1 334 amplicon sequence variants (ASVs~~) (richness) (Fehler: Verweis nicht gefunden).~~).

Alpha diversity of the active bacterial community, based on the RNA fraction, did not differ significantly between dry control and irrigated plots (Fig. 6). Diversity indices tended to be slightly higher in dry control plots than in irrigated plots, but this pattern was not statistically significant. Shannon diversity of the active community did not differ between treatments ($p = 0.956$).

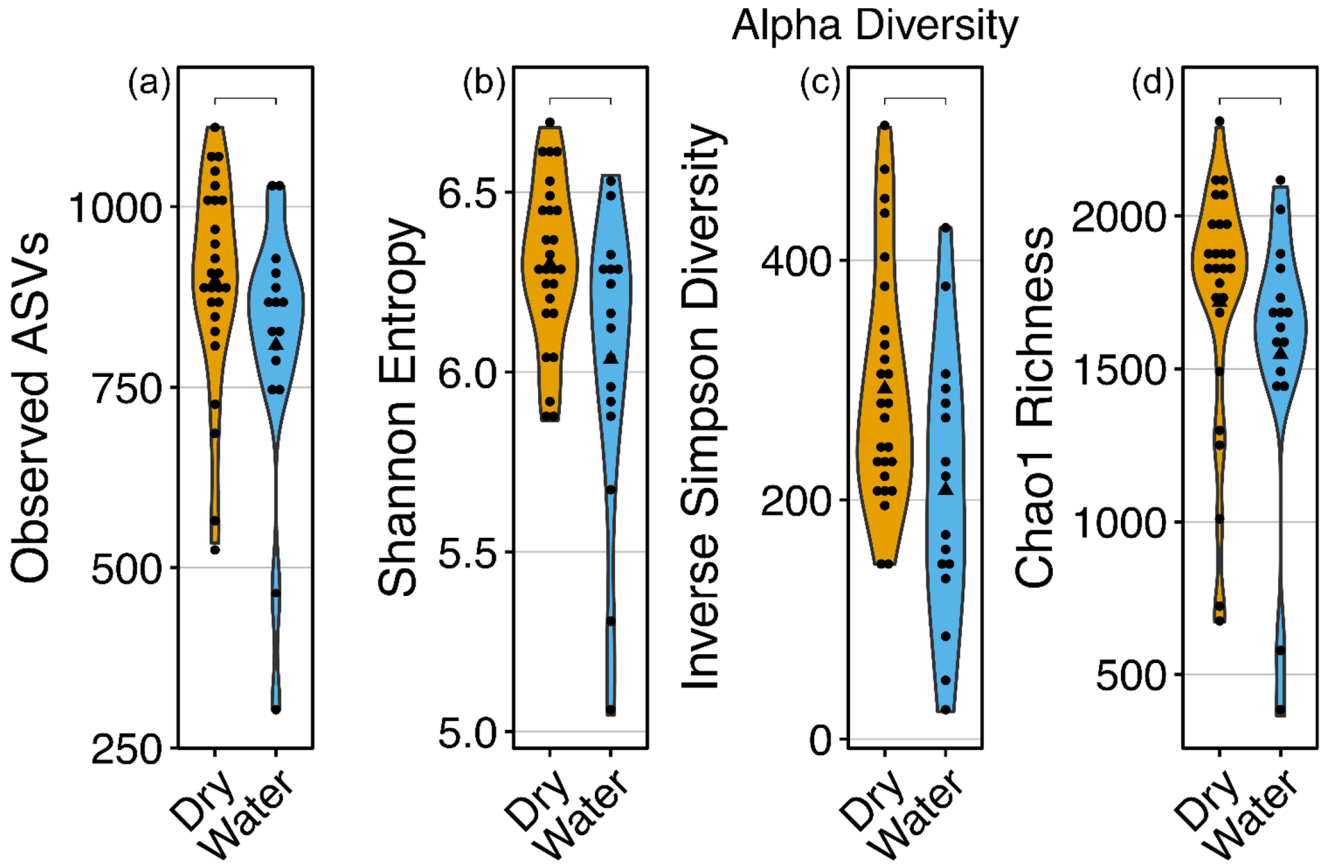


Figure ~~7~~6: ~~Observed~~Violin plots of observed amplicon sequence variants (ASVs~~) (~~; panel ~~(~~a~~)))~~ and ~~different~~ alpha diversity indices (panels ~~(~~b~~), (c) and (~~d~~))~~ of ~~microbial~~active bacterial communities ~~(~~based on the RNA~~) on~~ fraction in dry control plots (orange) and ~~watered~~irrigated plots (blue~~) plots.~~). Differences between ~~the~~ treatments were not significant ($p > 0.05$~~) (brackets without asterisk above violins).~~).

~~Microbial community composition of the different experimental treatments revealed high heterogeneity between sample plots. The soils~~Across all samples, the bacterial communities were dominated by ~~the phyla~~ Proteobacteria (~~mean: 17.4 % SD:±~~ 4.7~~), %),~~ Acidobacteriota (~~mean: 14.5 % SD:±~~ 4.9~~), %),~~ Actinobacteriota (~~mean: 13.5 % SD:±~~ 7.4~~) %),~~ and Verrucomicrobiota (~~mean: 11.5 % SD:±~~ 5.2~~). %).~~ These ~~were the most abundant~~ phyla ~~independent~~remained dominant irrespective of ~~wetting, soil~~treatment, depth, and ~~the day of the experiment~~sampling time (Appendix ~~F~~G). ~~At a finer taxonomic resolution~~At family level, Pedosphaeraceae (Verrucomicrobiota), unclassified Vicinamibacterales (Acidobacteriota), Xiphinematobacteraceae (Verrucomicrobiota~~))~~, and Nitrosomonadaceae (Gammaproteobacteria) were the ~~top four bacterial families found throughout all samples~~most abundant groups, with ~~the~~ mean relative abundances ~~varying between~~ranging from 3.2 to 4.6~~ and 3.2~~ %.

~~The common alpha diversity parameters (RNA-fraction) showed only minor differences between dry and wetted soils. Dry soils revealed a little higher diversity compared to the water treated soils (Fehler: Verweis nicht gefunden). The Shannon diversity of the active (RNA fraction) prokaryotic communities in dry and wet soils was not significantly different (p = 0.956). The DNA and RNA based community data suggest that microbial communities did not change with depth and treatment in terms of composition and active fractions within the short time frame of this study (14 days, Fehler: Verweis nicht gefunden).~~

Ordination of DNA- and RNA-based community composition showed no clear clustering by treatment or soil depth (Fig. 7). This indicates that neither total nor active bacterial community composition changed consistently in response to irrigation over the 14-day observation period.

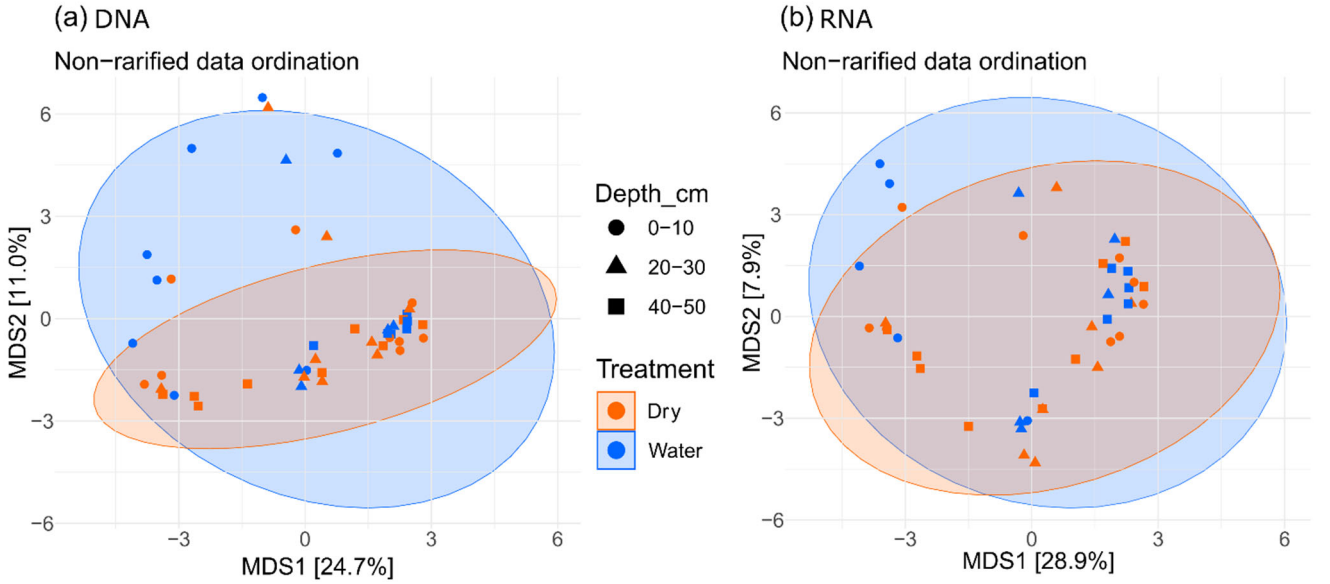


Figure ~~8~~7: Non-metric multidimensional scaling plots of ~~the microbial~~bacterial community composition ~~(a)~~based on ~~the~~ DNA ~~level~~ (a) and RNA (b~~) on the RNA level at three~~). Symbols indicate soil ~~depths (~~depth: 0–10 cm~~: dots,~~ (circles), 20–30 cm~~:~~ (triangles~~,~~), and 40–50 cm~~:~~ (squares~~) on dry~~). Colours indicate dry control plots (orange) and irrigated plots (blue~~) plots.~~).

~~The activities of the~~In contrast to community composition, extracellular ~~enzymes~~ enzyme activities responded clearly to irrigation and soil depth (Fig. 8). Activities of β-glucosidase, exochitinase, and acid phosphatase all decreased significantly with soil depth (p < 0.05~~) (Fehler: Verweis nicht gefunden).~~). β-glucosidase and exochitinase ~~showed~~activities were significantly higher ~~activities on wet~~in irrigated plots than ~~on~~in dry control plots (p < 0.05), whereas ~~the activity of~~ acid phosphatase activity did not ~~respond to the irrigation treatment~~differ between treatments (p > 0.05). ~~Time period~~ Sampling time after rewetting ~~by heavy rainfall~~ was not a significant factor for ~~all~~any of the three enzymes (p ~~<~~> 0.05~~), indicating that irrigation effects occurred very rapidly and did not recover to pre-treatment levels thereafter. The if non-significant interaction of treatment and soil depth (p < 0.05, two-way ANOVA) for~~). The stimulation of β-glucosidase and exochitinase ~~reflects that the wetting treatment effect (stimulation)~~by irrigation was strongest in ~~topsoils (0–5 cm)~~the upper soil layer and declined with depth~~.~~, as reflected by significant treatment × depth interactions for both enzymes (p < 0.05).

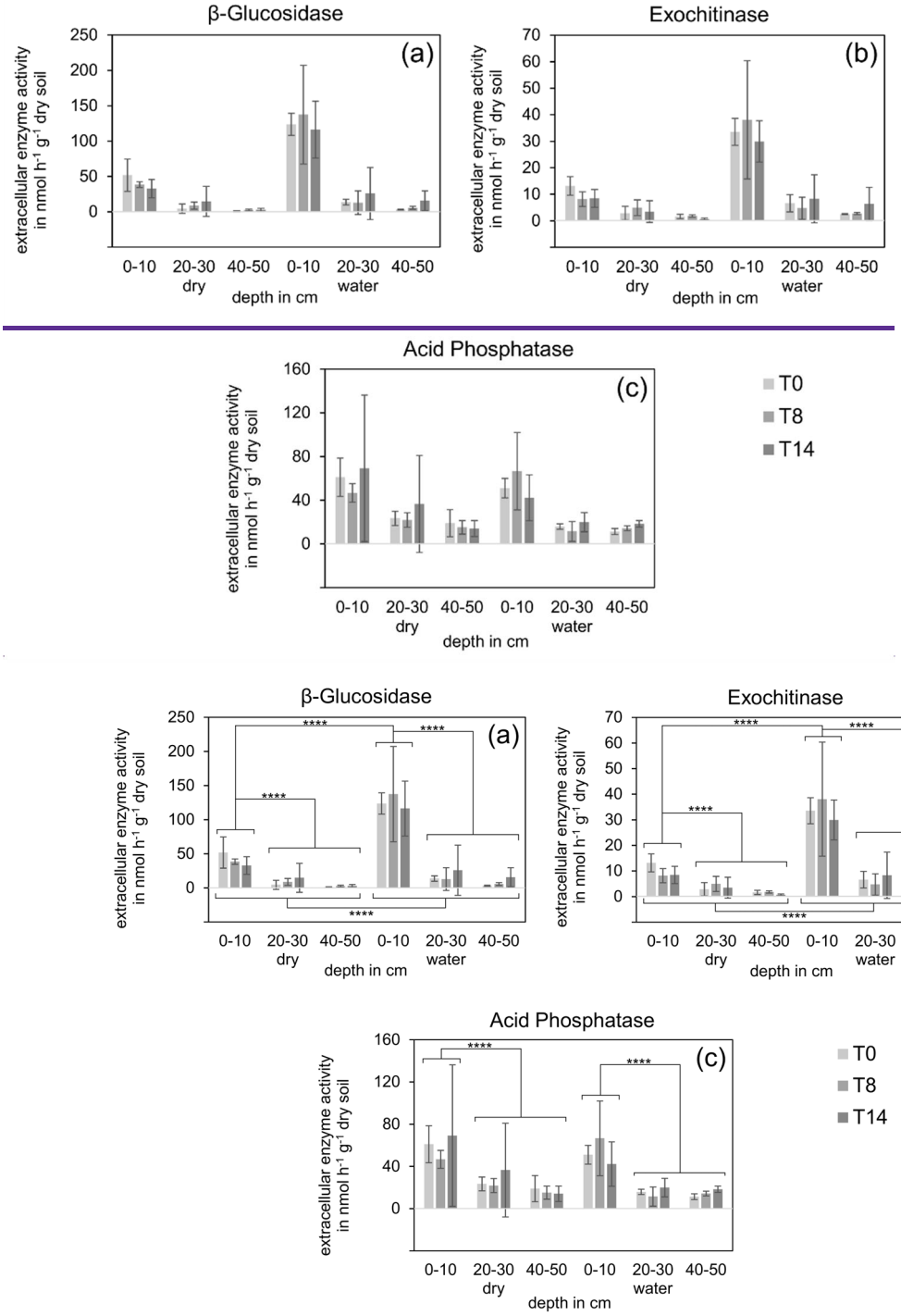


Figure ~~9~~8: Extracellular enzyme activities of β-glucosidase (~~panel (~~a~~)~~,), exochitinase (~~panel (~~b~~)~~), and acid phosphatase (~~panel (~~c~~)~~) at three soil depths ~~on~~in dry control and ~~watered~~irrigated plots. ~~The measurement time points day 0, 8 and 14 (~~Sampling times T0, T8, and T14~~)~~ are indicated by grey shading from light to dark. Error bars indicate standard deviations of three replicate plots. Significant treatment effects are indicated by asterisks (** = p < 0,0001).**

4 Discussion

4.1 ~~Water~~Preferential flow and ~~solute transport~~contrasting nitrate and ammonium redistribution

~~Both the water and the isotope mass balance showed that at T0 almost all of the irrigation water was recovered within the profile (Fehler: Verweis nicht gefundena and b). It is remarkable that shortly (2 h) after the simulated heavy rainfall, only about half of the irrigation water resided in the topsoil (0–20 cm) while the rest already had reached the subsoil (below 20 cm depth) (Fehler: Verweis nicht gefundena). This rapid deep infiltration was facilitated by the pronounced network of shrinkage cracks, which formed in the fine-textured soil due to the preceding drought (Schlögl et al., 2022).~~

The water mass balance (Fehler: Verweis nicht gefundena), following the recovery of the sum of irrigation water and precipitation throughout the whole experimental period (Irr_{tot}), showed that Irr_{tot} decreased from 96 % at T0 to 50 and 32 % at T8 and T14, respectively (Fehler: Verweis nicht gefundena). This strong loss of irrigation water can be rationalized by high evaporation rates (ETo = 4.2 mm day^{-1}, see Appendix E) during the course of the experiment. While during the simulated heavy rainfall at T0 (24.3 mm), parts of the irrigation water penetrated down to 50 cm soil depth or even deeper through shrinkage cracks, the continued daily irrigation scheme (5.2 mm day^{-1}) did not penetrate into the subsoil to a larger extent as the shrinkage cracks and thus the preferential flow paths disappeared after initial wetting as shown in Schlögl et al. (2022). Water of subsequent moderate daily irrigations was trapped near the soil surface and thus subject to high evaporation rates (4.2 mm day^{-1}). The pronounced impact of evaporation is supported by the isotope mass balance (Fehler: Verweis nicht gefundenb), which shows the recovery of the ^{2}H-labeled irrigation water from the simulated heavy rainfall event at T0, Irr_{HRE}. Over the entire 50 cm soil profile, the isotope mass balance indicates slightly lower losses than shown by the water mass balance but also indicates the most pronounced losses in the top 10 cm of the soil (56 % and 86 % at T8 and T14 compared to T0, respectively). Thus, the irrigation rate of 5.2 mm day^{-1} was not high enough to balance the losses by evapotranspiration and seepage during the experimental period as indicated by the decreasing values of the water mass balance with time.

The vertical distribution of ammonium (Fehler: Verweis nicht gefundena) and nitrate (Fehler: Verweis nicht gefundenb) on irrigated and dry plots was affected very differently by solute transport during the simulated heavy rainfall event. Nitrate as a weakly sorbing anion in soils is expected to travel in seepage water without noticeable retardation (Blume et al., 2016). Moreover, rapid transport of dissolved nitrate along preferential flow paths has been shown in earlier studies (Bronswijk et al., 1995; Kelly and Pomes, 1998) and could be the cause of initially decreasing nitrate contents in the topsoil in our experiment (loss of 0.37 mg nitrate-N in the top 20 cm) as evident by the comparison of nitrate in the soil profiles at DT0 (initial state) to WT0 (2 h after the heavy rainfall event) (Fehler: Verweis nicht gefundenb). However, even though D_2O-labeled water from the simulated heavy rainfall event was found in the subsoil two hours after the event and accompanying hydrological export of nitrate from the topsoil is very likely, we did not observe an accumulation of nitrate in the subsoil. Denitrification is probably not the reason for the disappearance of nitrate at WT0, since the redox potentials in the subsoil were still around 560 ± 30 mV two hours after the heavy rainfall simulation (Blume et al., 2016). Given that crops had been harvested before the start of the experiment and residual roots therefore were inactive, plant root uptake of nitrate (Cui and Caldwell, 1997) was likely not the cause for the profile-level decrease in nitrate mass. The gradual microbial immobilization of nitrate following severe drought within 2 hours of rewetting may have contributed, but cannot account for such large nitrate "losses". Moreover, this would occur at a time when the Birch effect indicates a flush of microbial metabolites and enzymes into the soil environment, i.e., loss of carbon and nitrogen mass from the microbial community rather than uptake and immobilization (nitrate). Therefore, the unaccounted nitrate was most likely transported below the zone investigated in this study (> 50 cm soil depth) via preferential flow. Directly beneath the upper 2 m clay layer, which comprises the investigated part of the soil profile, a shallow tufaceaous aquifer is located (Martin et al., 2020). The tufaceous aquifer is subject to moderately to strongly reducing conditions (Martin et al., 2020), so denitrification would occur, which could result in the formation of N_2O, a greenhouse gas, or the loss of inorganic nitrogen from the soil in the form of N_2 gas. Constant nitrate input in the groundwater would ultimately lead to a consumption of the reduction capacity of the tufa aquifer and thus to increasing nitrate concentrations in the aquifer. Therefore, nitrate leaching along preferential flow pathways during rewetting after drying can substantially threaten groundwater quality (Sánchez Pérez et al., 2003).

Ammonium (Fehler: Verweis nicht gefundena) is subject to cation exchange at negatively charged mineral surfaces including clay minerals. Ammonium therefore is less prone to (downward) transport in soils compared to nitrate (Blume et al., 2016). This retardation prevented the rapid loss of ammonium from the topsoil due to percolation of the irrigation water. The low mobility of ammonium in the soil profile was confirmed when comparing the ammonium mass profiles at DT0 (initial state)

to WT0 (2 h after the heavy rain event, Fehler: Verweis nicht gefundena) with very similar total ammonium contents and depth distributions in both.

4.2 Nitrogen turnover processes

Soil nitrate and ammonium contents showed a high variability between the three replicate experimental plots; thus, the trends observed in space and time were often not statistically significant (Fehler: Verweis nicht gefunden). This reflects the high spatial heterogeneity of the distribution of inorganic nitrogen compounds in soils that was also observed by Hergert et al. (1995). At our field site, the heterogeneous distribution (quantified in terms of coefficients of variation) of the simulated heavy rainfall event water was governed by the presence of shrinkage cracks (Schlögl et al., 2022). In the beginning of the experiment, pronounced cracks (up to 1 cm width) were visible at the soil surface and the coefficients of variation of deuterium enrichment of soil water were high. These cracks closed in later states of the experiment while the coefficients of variation of isotope signatures decreased. The coefficients of variation of nitrate and ammonium, however, showed different patterns (Appendix G). For nitrate, the coefficients of variation on the W plots in the top 10 cm were much lower on day 0 than on day 6 and day 14 (Appendix G), reflecting the opposite trend in variance as for the deuterium enrichment of soil water. For ammonium, no clear trends of the coefficients of variation existed in space and time. The spatial and temporal heterogeneity of the distribution of ammonium and nitrate was therefore not governed by the presence of shrinkage cracks.

The irrigation of dry soil stimulated the mineralization of organic nitrogen (N_{org}) which is reflected by the doubling of ammonium concentration in the topsoil (0–5 cm depth) from DT0 to WT0 (Fehler: Verweis nicht gefundena). This increase is in line with the observations made by H. Birch, who described intense nitrogen release upon rewetting of dry soils (Birch, 1958, 1960). The Birch effect is induced by the mineralization of dead microbial biomass and of osmoregulatory substances that are released by microorganisms upon rewetting (Fierer and Schimel, 2002; Jarvis et al., 2007; Saetre and Stark, 2005; Unger et al., 2010). This is supported by the significant and immediate increase of two extracellular enzymes (β-glucosidase and exochitinase) in soils of W plots compared to D plots within two hours of heavy rainfall simulation (Fehler: Verweis nicht gefunden), which indicates the release of intracellular compounds (including enzymes) by lysis of a fraction of the microbial cells due to irrigation (Khan et al., 2019). The prolonged increase of ammonium in the topsoil at T6 and T14 (0.05 mg ammonium-N and 0.10 mg ammonium-N, respectively) can be explained by continued net mineralization of organic matter in cropland soils (Booth et al., 2005), by bulk atmospheric deposition of ammonium (average of 0.011 mg ammonium-N per week on the cross sectional area of a sample core (Beyn et al., 2014), for calculation see Appendix H) and by further nitrogen release due to daily drying and rewetting (Birch, 1958; Fierer and Schimel, 2002). Nitrogen fixation as a potential ammonium source was likely negligible, as no legumes were grown at this field site prior to the experiment. At a soil depth of 10 cm and below, ammonium contents, however, did not respond much to irrigation. The reasons can be that (i) there is less labile organic matter at soil depths below 10 cm (Appendix B) and thus less ammonium can be released from mineralization of organic compounds or (ii) that most ammonium present is strongly sorbed to clay minerals and thus is not accessible for nitrification or other microbial-driven processes (Buss et al., 2004; Cavalli et al., 2015). Ammonium can either be bound as exchangeable cation on clay minerals (Blume et al., 2016; Buss et al., 2004) or it can enter the 2:1 clay mineral interlayer (Buss et al., 2004), rendering interlayer ammonium largely recalcitrant to microbial utilization. The high clay and silt content of the studied soils (Appendix C) highlights the high cation-exchange capacity triggered by high surface area and high negative charge density of the clays for ammonium sorption. Alternatively, (iii) ammonium contents can remain relatively constant if the ammonium that is produced per time step is consumed by microbial uptake or oxidized to nitrate under oxic conditions during the same period. On the W plots, the increase of nitrate mass in the topsoil (0–5 cm) from T0 to T6 and to T14 (by 0.061 mg nitrate-N and 0.05 mg nitrate-N, respectively) (Fehler: Verweis nicht gefundenb) cannot fully be explained by bulk atmospheric nitrate deposition (0.007 mg nitrate-N per week on the cross sectional area of a sample core (Beyn et al., 2014) for calculation see Appendix I). The increase of nitrate mass at 0–20 cm soil depth at T6 and below 20 cm depth at T14 (Fehler: Verweis nicht

gefundenb) can thus be explained by nitrification (oxidation) of ammonium under oxic conditions (Fehler: Verweis nicht gefunden) (Cui and Caldwell, 1997). The redox potentials in W plots showed great variations at 10 and 20 cm depth (Fehler: Verweis nicht gefundena and b), which occurred between sensors (spatial variations) and between times in single sensors (temporal variations) (Fehler: Verweis nicht gefundenb). The spatial variations can be explained by oxic and anoxic microsites in otherwise anoxic and oxic environments, respectively (Dorau et al., 2023; Kuzyakov and Blagodatskaya, 2015). Moderate daily fluctuations (e.g., at all sensors at 5 cm), were potentially induced by temperature changes (Dorau et al., 2021). The stronger temporal variations (e.g., sensor 1 at 10 cm (Fehler: Verweis nicht gefundena)) followed the daily irrigation and were thus most likely the result of rapid changes between air- and water-filled pore space. Following these changes in oxygen availability, the nitrification rates likely fluctuated. For most of the experimental time, the redox conditions remained above +100 mV, a threshold above which nitrification is active (Hansen et al., 1981), and during these periods we observed an increase in nitrate mass at 5–10 cm and 10–20 cm soil depth at T6 (Figure 5b). Below 20 cm depth at T6, nitrification did not substantially occur because redox potentials (Fehler: Verweis nicht gefunden) were below +100 mV, disfavouring the process. At T14, however, due to the pause in daily light irrigation from the T10 to T14, redox potentials below 20 cm depth rose above the threshold for nitrification related to increasing nitrate contents at T14. Nitrate and ammonium mass changes were therefore partially coupled and nitrate accumulation under oxic conditions was related to ammonium draw-down and/or continued mineralization of N_{org} across the whole soil profile.

In summary, the observed nitrogen turnover processes were initially governed by the rewetting of the dry soil and the so-called "Birch effect", which is known to be a short term effect (Birch, 1958; Cui and Caldwell, 1997; Unger et al., 2010). After approximately one week of the experiment, the nitrogen turnover processes switched from the pulse driven regime after rewetting to the "usual" redox driven nitrogen cycling regime governed by oxygen availability as reflected by the drop of in situ redox potentials at greater depth.

The 1.5 fold and 2.5 fold increase of ammonium and nitrate, respectively, on D plots between T0 and T14 is remarkable. Temperatures below the plastic foil may have increased, activating microbial turnover processes, although we did not observe a shift in microbial community composition in the D plots on T14. Prolonging the experimental drought period prior to irrigation of the dry plots by another two weeks, such as happened on the D plots, might have critically amplified the drying effects on microbial functioning, and therefore have induced a stronger cellular water deficit and soil microbial turnover and death, with concomitant releases of organic and inorganic nitrogen (Fehler: Verweis nicht gefunden). Alternatively, constant evaporation on the D plots during the experimental period might have induced the rise of soil water transporting dissolved species such as nitrate upwards. On the W plots, this effect was interrupted by the recurring irrigation.

4.3 Microbial communities and activities

Environmental conditions such as temperature, pH, oxygen availability and moisture directly influence soil microbes and thereby affect biogeochemical processes such as nitrogen turnover. The use of stable isotope labelled substrates has shown that soil microbial communities consist of a dynamic fraction that can be activated by rewetting (Aanderud et al., 2015). Revealing these processes and changes in community structure remains challenging. Nucleic acids can persist in the soil environment for long time spans (Carini et al., 2016) hampering diversity estimations. This "inactive" DNA in environmental samples has been linked to either dormant cells (Aanderud et al., 2015) resembling a seed bank or to extracellular nucleic acids that may play a role in other processes (Lennon et al., 2018). In this study, the more short-lived RNA has been used as a proxy of the "active" microbial community fraction. However, we did not find any significant differences between sampling treatments, depth or the length of the experiment (Fehler: Verweis nicht gefunden). Populations of soil bacteria vary over space, time and in response to environmental changes. Their spatial variation can occur at the micro-scale (Vos et al., 2013), in relation to soil microstructure and organic matter distribution and thus it can be difficult to depict differences between

~~samples. The increase in activities of the extracellular enzymes β-glucosidase and exochitinase (Fehler: Verweis nicht gefunden) and of ammonium (Fehler: Verweis nicht gefunden) on W plots nevertheless indicated an activation of microbial cells by the rewetting.~~

~~In dry soils, microbial communities display reduced metabolic activity due to a combination of desiccation stress and reduced substrate diffusion (Schimel et al., 2007). Our data indicate a higher microbial diversity in the dry soils (RNA) than in the irrigated plots (Fehler: Verweis nicht gefunden), although the differences in diversity were not significant. While rainfall and rewetting of soils have been shown to increase microbial metabolism (Blazewicz et al., 2014; Fierer and Schimel, 2002) they can also exert stress to the microbial communities (Barnard et al., 2013; Schimel, 2018), resulting in the elimination of microbial taxa not adapted to dry-wet cycles (Armstrong et al., 2016; Fierer et al., 2003; Veach and Zeglin, 2020). The microbial communities in our tested soils were not particularly pre-adapted to drought and rewetting – so such a functional selection process within the different taxa present during soil rewetting seems implausible. The reasons for this selection process – from microbial death to soil chemistry as a driver – are still under debate (Schimel, 2018). In our experiment, the induced osmotic stress most likely drove the microbial community shift.~~

~~5 Conclusions~~

~~Due to climate change, the frequency of droughts and heavy precipitation events is increasing in temperate climates. In our study, we investigated the effects of a heavy rainfall event after a summer drought in a loamy floodplain soil on (i) water flow and solute transport of inorganic nitrogen species, (ii) the occurrence of the Birch effect and the transition towards redox-driven nitrogen turnover processes, and (iii) soil microbial community structure.~~

~~Our study showed, that (a) during the heavy rainfall event, water including dissolved nitrate infiltrated into the subsoil along preferential flow paths. This carries the risk of nitrate leaching into the underlying aquifer. (b) Upon rewetting, an increase in inorganic nitrogen (ammonium) occurred as described by the Birch effect. The study confirms that this effect is a short-term effect, lasting a few days at the most until the normal redox-driven nitrogen cycling becomes dominant again. (c) Soil microbial community composition did not respond much to irrigation at both DNA and RNA levels. However, lower diversity indices on irrigated vs. dry plots indicate that stress induced by rewetting lead to some shift in the microbial community towards better adapted taxa. The leaching of nitrate into shallow aquifers upon heavy rainfall events and the shift of the microbial community in cropland soils of Central Europe should be investigated in more detail in follow-up studies.~~

The combined water and isotope mass balances showed that the simulated heavy rainfall event caused rapid infiltration throughout the sampled 0–50 cm profile. Two hours after irrigation, only about half of the recovered water was retained in the upper 20 cm, whereas a substantial fraction had already reached deeper soil layers (Fig. 3a). The δ^2H isotope mass balance confirmed that D_2O-~~labelled~~labeled heavy-rainfall water was distributed across the entire sampled profile shortly after irrigation (Fig. 3b). This rapid deep infiltration is consistent with preferential flow through the pronounced shrinkage-crack network that formed in the fine-textured soil during the preceding drought period (Schlögl et al., 2022).

The hydrological response changed markedly after the initial wetting. During the subsequent phase of recurrent moderate irrigation, the apparent recovery of total water input within the sampled profile decreased from 96 % at T0 to 50 % at T6 and 32 % at T14 (Fig. 3a). At the same time, newly added water was retained mainly in the upper soil layers. This pattern indicates that the initial heavy rainfall event used open shrinkage cracks as preferential flow paths, whereas later moderate irrigation occurred after crack closure and therefore infiltrated more slowly into the soil matrix. Because the plots had been harvested before the experiment, water losses were likely driven mainly by evaporation and drainage below the sampled profile rather than by plant transpiration. The calculated ET_0 of 4.2 mm day^{-1} therefore represents atmospheric evaporative demand rather than plot-scale evapotranspiration. The stronger decline in ~~labelled~~labeled-water recovery from the uppermost 10 cm compared with deeper layers further supports strong near-surface water loss after the initial event.

Nitrate and ammonium responded differently to this hydrological redistribution. Nitrate mass decreased strongly in the upper soil layers within two hours after the simulated heavy rainfall event, whereas ammonium mass did not show comparable profile-level losses (Fig. 5). This contrast is consistent with the different mobility of the two inorganic nitrogen species. Nitrate is weakly sorbed and can be transported rapidly with percolating and infiltrating water, whereas ammonium is retained more strongly by cation exchange at negatively charged mineral surfaces, particularly clay minerals (Blume et al., 2016). Thus, preferential flow after drought likely caused rapid vertical nitrate displacement, while ammonium remained largely retained in the sampled soil profile.

The decrease in nitrate mass in the upper soil profile was not accompanied by a corresponding nitrate accumulation at 30–50 cm depth. This suggests that at least part of the displaced nitrate may have moved below the sampled 50 cm profile. Alternative explanations, such as denitrification or plant uptake, are less likely to fully explain the immediate nitrate decrease. Redox potentials were still oxidizing shortly after the simulated heavy rainfall event, and crops had been harvested before the experiment. Microbial immobilization may have contributed, but the rapid timing and magnitude of the nitrate decrease are more consistent with hydrological export along preferential flow paths. Nevertheless, because nitrate was not measured below 50 cm depth, nitrate transfer beyond the sampled profile should be interpreted as a likely but indirect inference.

The potential transfer of nitrate below the biologically active topsoil is relevant for groundwater quality, particularly in fine-textured floodplain soils, where shrinkage cracks can bypass the soil matrix. The study site is underlain by a shallow tufa aquifer below the upper clay-rich layer (Martin et al., 2020). If nitrate reaches such deeper zones repeatedly, its fate will depend on the local redox status and denitrification capacity of the subsurface. Therefore, heavy rainfall following drought may represent a short but important hydrological window during which nitrate can bypass retention and transformation in the upper soil profile.

4.2 Inorganic nitrogen pools after rewetting: evidence for a short-term rewetting pulse and redox-associated nitrate dynamics

The increase in ammonium mass in the uppermost soil layer shortly after irrigation is consistent with a rewetting-induced mineralization pulse, commonly referred to as the Birch effect. Ammonium mass nearly doubled in the 0–5 cm layer within two hours after the simulated heavy rainfall event (Fig. 5a). This response agrees with earlier observations that rewetting of dry soils can cause a transient release of inorganic nitrogen through microbial cell lysis, mineralization of dead microbial biomass, and decomposition of osmoregulatory compounds released during drought and rewetting (Birch, 1958, 1960; Fierer and Schimel, 2002; Jarvis et al., 2007; Saetre and Stark, 2005; Unger et al., 2010). The simultaneous increase in β-glucosidase and exochitinase activities supports the interpretation that rewetting rapidly stimulated microbial and enzymatic activity in the topsoil. The increase in ammonium mass cannot solely be caused by atmospheric deposition (Appendix I).

Below 5 cm depth, ammonium masses changed only weakly in irrigated plots. Three, non-exclusive mechanisms may explain this limited response. First, labile organic matter decreased with depth (Appendix B), reducing the potential for rewetting-induced ammonium release. Second, ammonium may have been retained by sorption to clay minerals and partly fixed in 2 : 1 clay interlayers, reducing its mobility and microbial accessibility (Buss et al., 2004; Cavalli et al., 2015). Third, newly produced ammonium may have been balanced by microbial uptake or oxidation under locally oxic conditions. Because gross nitrogen transformation rates were not measured, these mechanisms cannot be separated quantitatively.

Nitrate dynamics after the initial rainfall event were more complex. After the immediate decline in nitrate mass at T0, total nitrate mass in irrigated plots increased again by T14 (Fig. 5b). This increase cannot be fully explained by atmospheric nitrate deposition, which was small relative to the observed nitrate changes (Appendix J). Periods with higher redox potentials may have favoured nitrification, whereas lower redox potentials may have favoured nitrate reduction. The redox records

support this interpretation qualitatively: redox potentials declined after irrigation but showed strong temporal variation, particularly at 10–30 cm depth, and increased again during the interruption of daily irrigation between T10 and T14 (Fig. 4).

However, these data do not allow direct quantification of nitrification, denitrification, immobilization, or mineralization rates. Therefore, we interpret the observed nitrate patterns as redox-associated changes in inorganic nitrogen pools, not as direct evidence for a process-level switch in nitrogen cycling. This distinction is important because nitrate and ammonium pool sizes integrate multiple simultaneous processes, including production, consumption, immobilization, and transport. In addition, redox potentials were measured with high temporal resolution but only in one irrigated and one dry control plot. The sometimes very marked differences in the sensors' responses can be caused, for example, by the highly uneven distribution of dry cracks or remaining root fragments from the harvested plants. The redox data therefore provide valuable mechanistic context, but spatial extrapolation to all replicate plots must remain cautious.

The strong spatial and temporal variability in nitrate and ammonium masses further highlights the difficulty of inferring nitrogen process rates from pool-size data alone. Coefficients of variation (Appendix H) showed that inorganic nitrogen distributions did not simply mirror the spatial pattern of the D_2O~~δ^2H labelled~~labeled water. While preferential flow clearly governed rapid water redistribution during the initial event, nitrate and ammonium masses were also shaped by sorption, biological transformations, and local soil heterogeneity. Thus, drought-induced cracks were important for rapid water and nitrate displacement, but they were not the only control on inorganic nitrogen pool distributions during the subsequent 14 days.

The increase in ammonium and nitrate masses in dry control plots between T0 and T14 also illustrates this interpretive complexity. Because these plots remained dry for longer, continued drought may have intensified microbial stress and contributed to organic matter and microbial biomass turnover, with subsequent accumulation of inorganic nitrogen. In addition, evaporation may have promoted upward redistribution and concentration of dissolved nitrate in the upper soil layers. The temporary plastic cover used to exclude natural rainfall may also have altered temperature and moisture conditions near the soil surface. These explanations remain tentative, but they emphasize that inorganic nitrogen pools can change substantially even without experimental irrigation.

Overall, the nitrogen data support two main conclusions. First, rewetting caused a rapid but spatially restricted ammonium increase in the topsoil, consistent with a short-term Birch-effect response. Second, nitrate pools after the initial event were associated with changing hydrological and redox conditions, but the underlying process rates cannot be resolved without direct measurements of gross mineralization, nitrification, immobilization, and denitrification.

4.3 Microbial community composition and extracellular enzyme activities

Microbial responses to drought and rewetting differed between community composition and extracellular enzyme activity. Bacterial community composition showed no consistent treatment-related separation at either the DNA or RNA level during the 14-day experiment (Fig. 7). Alpha diversity of the active community also did not differ significantly between dry control and irrigated plots (Fig. 6). These results indicate that the short-term rewetting event did not cause a detectable restructuring of bacterial community composition at the taxonomic resolution captured by 16S rRNA amplicon sequencing.

The absence of a clear compositional response does not imply that microorganisms were inactive. In contrast, β-glucosidase and exochitinase activities increased significantly in irrigated plots, especially in the upper soil layer (Fig. 8). This indicates that rewetting rapidly affected microbial activity or extracellular enzyme availability, even though community composition remained comparatively stable. Such a decoupling between microbial activity and community composition is plausible because enzyme activities can respond within hours to changes in water availability, substrate diffusion, cell lysis, and microbial metabolic activation, whereas detectable shifts in community composition may require longer time scales or stronger selective pressure.

Several factors may explain why microbial community composition remained stable. First, floodplain and arable soils are highly heterogeneous at small spatial scales, and such micro-scale variability can mask treatment effects in community

ordinations (Vos et al., 2013). Second, DNA can persist in soils as relic DNA or in dormant cells, which may obscure short-term changes in the living community (Carini et al., 2016; Lennon et al., 2018). Although RNA was ~~analysed~~analyzed as a proxy for the active community, rRNA-based community profiles may still reflect both activity and standing ribosome pools rather than instantaneous growth or process rates. Third, the 14-day observation period may have been too short to detect consistent taxonomic restructuring, particularly if the community response was mainly physiological.

The slightly higher RNA-based diversity indices in dry control plots than in irrigated plots were not statistically significant and should therefore not be interpreted as evidence for selection of better-adapted taxa. Rewetting can impose osmotic stress and can eliminate sensitive cells, while also stimulating dormant or rare taxa (Aanderud et al., 2015; Barnard et al., 2013; Blazewicz et al., 2014; Schimel, 2018). However, our data provide stronger evidence for an activity response than for compositional selection. Therefore, the microbial results are best interpreted as showing rapid functional activation after rewetting without detectable community restructuring over the short experimental period.

This interpretation is consistent with the enzyme and nitrogen results. Increased β-glucosidase and exochitinase activities after irrigation indicate enhanced potential for C and N acquisition from organic substrates and support the observed short-term ammonium increase in the topsoil. In contrast, the lack of a clear microbial community shift suggests that the immediate biogeochemical response was driven primarily by altered microbial activity, substrate accessibility, and physical–chemical conditions rather than by major changes in bacterial community composition.

5 Conclusions

Heavy rainfall after summer drought caused rapid preferential infiltration through drought-induced shrinkage cracks in this fine-textured floodplain soil. Within two hours, D_2O ~~labelled~~labeled water reached at least 50 cm depth, and nitrate mass declined in the upper soil profile without accumulating in the sampled subsoil, suggesting possible nitrate transport below 50 cm. In contrast, ammonium was largely retained within the soil profile and increased only in the uppermost layer, consistent with a short-term rewetting-induced mineralization pulse. Subsequent moderate irrigation was retained mainly in the topsoil, most likely because shrinkage cracks had closed after initial wetting. Redox potentials declined strongly after irrigation and were associated with later changes in nitrate pools, but these patterns cannot be interpreted as direct estimates of nitrogen transformation rates. Microbial community composition remained stable at both DNA and RNA levels, whereas β-glucosidase and exochitinase activities increased after irrigation, indicating rapid functional activation rather than detectable community restructuring. These findings show that heavy rainfall after drought can create a brief but important window for nitrate displacement through preferential flow pathways, potentially bypassing nitrogen retention in the biologically active topsoil and increasing nitrate transfer to deeper soil layers or shallow groundwater. The study, conducted under realistic field conditions, demonstrated that the interaction of the processes under investigation is complex and that, for example, the exact mechanisms of nitrogen cycling could not be adequately explained using the chosen approach. Future work should combine tracer-based hydrology with direct measurements of gross nitrogen transformation rates to disentangle transport from microbial nitrogen cycling during drought–rewetting events.

Data availability

The data presented in this paper are published in the database of the project "CAMPOS – Catchments as Reactors" at the University of Tübingen, available online (~~LINK~~https://doi.org/10.57754/FDAT.qz8p1-3dr53).

Gene amplicon sequencing data, generated by the JMF under Project IDsJMF-2006-4 and JMF-2010-08, were deposited under the BioProject accession number PRJEB87326.

~~Sample availability?~~

~~Supplement link~~

Author contributions

Johanna Schlögl: Conceptualization, Methodology, Investigation, Data curation, Formal analysis, Validation, Visualization, Writing – original draft preparation; Clemens Karwautz: For the data on microbial community composition: Data curation, Formal analysis, Visualization, Writing – original draft preparation; Lena Cramaro: Conceptualization, Methodology, Investigation (data on microbial community composition), Data curation (data on microbial community composition); Wolfgang Wanek: Investigation (extracellular enzyme activities), Formal analysis (extracellular enzyme activities), Writing – review and editing; Judith Prommer: Sample analysis (extracellular enzyme activities), Writing – review and editing; Theresa Böckle: Sample analysis (extracellular enzyme activities), Writing – review and editing; Andreas Kappler: Funding acquisition, Writing – review and editing; Stefan B. Haderlein: Conceptualization, Methodology, Funding acquisition, Project administration, Resources, Writing – review and editing; Christian Griebler: Conceptualization, Methodology, Funding acquisition, Project administration, Resources, Writing – review and editing.

Competing interests

The authors declare that they have no conflict of interest.

Acknowledgements

Financial support was provided by the German Research Foundation by the Collaborative Research Center 1253 CAMPOS Grant Agreement SFB 1253/1 2017 (Project 4: Floodplain Biogeochemistry and Project 6: Controls for the Fate of Agrochemicals in Soils).

We acknowledge the help of M. Jantz during the preparation of the field experiment, of M. Jantz, T. Siller, F. Straub and D. Sanchez Anaya for assistance during the field work, of M. Engelhardt for analyses of soil texture and total organic carbon and for assistance with the extraction of inorganic nitrogen species, and of H. Schulz for freeze drying of soil samples (all from University of Tübingen). We thank C. Stumpp (University of Natural Resources and Life Sciences, Vienna) for the analysis of soil water stable isotopes and the assistance with the data evaluation, S. Klingler and S. Martin (both University of Tübingen) for providing information on and a photo of one of their cores taken in the Ammer valley, and the landowner for permission to conduct the field work on his farmland.

References

Aanderud, Z. T., Jones, S. E., Fierer, N., and Lennon, J. T.: Resuscitation of the rare biosphere contributes to pulses of ecosystem activity, Frontiers in Microbiology, 6, 10.3389/fmicb.2015.00024, 2015.

Agrarmeteorologie Baden-Württemberg: Wetterdaten, Station Unterjesingen: https://www.wetter-bw.de/Internet/AM/NotesBwAM.nsf/bwweb/4262596897754529c1257ca8002f9d19?OpenDocument, last access: 14.10.2021.

Allen, R. G., Pereira, L. S., Raes, D., and Smith, M.: FAO Irrigation and drainage paper 56 - Crop evapotranspiration - Guidelines for computing crop water requirements, FAO - Food and Agriculture Organization of the United Nations, Rome1998.

American Meteorological Society: "Rain". Glossary of Meteorology: https://glossary.ametsoc.org/wiki/Rain, last access: 03.02.2024.

Armstrong, A., Valverde, A., Ramond, J.-B., Makhalanyane, T. P., Jansson, J. K., Hopkins, D. W., Aspray, T. J., Seely, M., Trindade, M. I., and Cowan, D. A.: Temporal dynamics of hot desert microbial communities reveal structural and functional responses to water input, Scientific Reports, 6, 34434, 10.1038/srep34434, 2016.

Baldwin, D. S. and Mitchell, A. M.: The effects of drying and re-flooding on the sediment and soil nutrient dynamics of lowland river–floodplain systems: a synthesis, Regulated Rivers: Research & Management, 16, 457-467, https://doi.org/10.1002/1099-1646(200009/10)16:5<457::AID-RRR597>3.0.CO;2-B, 2000.

Barnard, R. L., Osborne, C. A., and Firestone, M. K.: Responses of soil bacterial and fungal communities to extreme desiccation and rewetting, The ISME Journal, 7, 2229-2241, 10.1038/ismej.2013.104, 2013.

Beven, K. and Germann, P.: Macropores and water flow in soils revisited, Water Resources Research, 49, 3071-3092, https://doi.org/10.1002/wrcr.20156, 2013.

Beyn, F., Matthias, V., and Dähnke, K.: Changes in atmospheric nitrate deposition in Germany – An isotopic perspective, Environmental Pollution, 194, 1-10, https://doi.org/10.1016/j.envpol.2014.06.043, 2014.

Birch, H. F.: The effect of soil drying on humus decomposition and nitrogen availability, Plant and Soil, 10, 9-31, 10.1007/BF01343734, 1958.

Birch, H. F.: Nitrification in soils after different periods of dryness, Plant and Soil, 12, 81-96, 10.1007/BF01377763, 1960.

Blazewicz, S. J., Schwartz, E., and Firestone, M. K.: Growth and death of bacteria and fungi underlie rainfall-induced carbon dioxide pulses from seasonally dried soil, Ecology, 95, 1162-1172, https://doi.org/10.1890/13-1031.1, 2014.

Blume, H.-P., Brümmer, G. W., Fleige, H., Horn, R., Kandeler, E., Kögel-Knabner, I., Kretzschmar, R., Stahr, K., and Wilke, B.-M.: Scheffer/Schachtschabel Soil Science, Springer, Berlin, Heidelberg, Berlin, Heidelberg, XVIII, 618 pp., https://doi.org/10.1007/978-3-642-30942-7, 2016.

~~Booth, M. S., Stark, J. M., and Rastetter, E.: CONTROLS ON NITROGEN CYCLING IN TERRESTRIAL ECOSYSTEMS: A SYNTHETIC ANALYSIS OF LITERATURE DATA, Ecological Monographs, 75, 139-157, https://doi.org/10.1890/04-0988, 2005.~~

Bronswijk, J. J. B., Hamminga, W., and Oostindie, K.: Rapid nutrient leaching to groundwater and surface water in clay soil areas, European Journal of Agronomy, 4, 431-439, https://doi.org/10.1016/S1161-0301(14)80095-6, 1995.

Buss, S., Herbert, A., Morgan, P., Thornton, S., and Smith, J.: A Review of Ammonium Attenuation in Soil and Groundwater, Quarterly Journal of Engineering Geology and Hydrogeology - Q J ENG GEOL HYDROGEOL, 37, 347-359, 10.1144/1470-9236/04-005, 2004.

Callahan, B. J., McMurdie, P. J., and Holmes, S. P.: Exact sequence variants should replace operational taxonomic units in marker-gene data analysis, The ISME Journal, 11, 2639-2643, 10.1038/ismej.2017.119, 2017.

Carini, P., Marsden, P. J., Leff, J. W., Morgan, E. E., Strickland, M. S., and Fierer, N.: Relic DNA is abundant in soil and obscures estimates of soil microbial diversity, Nature Microbiology, 2, 16242, 10.1038/nmicrobiol.2016.242, 2016.

Cavalli, D., Consolati, G., Marino, P., and Bechini, L.: Measurement and simulation of soluble, exchangeable, and non-exchangeable ammonium in three soils, Geoderma, 259-260, 116-125, https://doi.org/10.1016/j.geoderma.2015.05.011, 2015.

Coby, A. J., Picardal, F., Shelobolina, E., Xu, H., and Roden, E. E.: Repeated anaerobic microbial redox cycling of iron, Appl Environ Microbiol, 77, 6036-6042, 10.1128/AEM.00276-11, 2011.

Coumou, D. and Rahmstorf, S.: A decade of weather extremes, Nature Climate Change, 2, 491-496, 10.1038/nclimate1452, 2012.

Cui, M. and Caldwell, M. M.: A large ephemeral release of nitrogen upon wetting of dry soil and corresponding root responses in the field, Plant and Soil, 191, 291-299, 10.1023/A:1004290705961, 1997.

DIN Deutsches Institut für Normung e. V.: DIN EN ISO 17892-4 Geotechnical investigation and testing - Laboratory testing of soil - Part 4: Determination of particle size distribution, Beuth, Berlin, 7, 2017.

~~Dorau, K., Bohn, B., Weihermüller, L., and Mansfeldt, T.: Temperature-induced diurnal redox potential in soil, Environmental Science: Processes & Impacts, 23, 1782-1790, 10.1039/D1EM00254F, 2021.~~

~~Dorau, K., Uteau, D., Maisch, M., Kappler, A., Peth, S., and Mansfeldt, T.: Redoxtrons – An experimental system to study redox processes within the capillary fringe, European Journal of Soil Science, 74, e13347, https://doi.org/10.1111/ejss.13347, 2023.~~

Durner, W., Iden, S. C., and von Unold, G.: The integral suspension pressure method (ISP) for precise particle-size analysis by gravitational sedimentation, Water Resources Research, 53, 33-48, https://doi.org/10.1002/2016WR019830, 2017.

Fierer, N. and Schimel, J. P.: Effects of drying–rewetting frequency on soil carbon and nitrogen transformations, Soil Biology and Biochemistry, 34, 777-787, https://doi.org/10.1016/S0038-0717(02)00007-X, 2002.

Fierer, N., Schimel, J. P., and Holden, P. A.: Influence of Drying–Rewetting Frequency on Soil Bacterial Community Structure, Microbial Ecology, 45, 63-71, 10.1007/s00248-002-1007-2, 2003.

German Meteorological Service (DWD): Monatliche Mittel/Summen, Niederschlag, Station Stuttgart-Echterdingen: https://www.dwd.de/DE/leistungen/kvo/baden_wuerttemberg.html?nn=480164, last access: 02.02.2024.

Geyer, O. F., Gwinner, M. P., Geyer, M., and Ellwanger, D.: Geologie von Baden-Württemberg, 5., völlig neu bearb. Aufl. / hrsg. von Matthias Geyer ... unter Mitarb. von Dietrich Ellwanger ... Schweizerbart, Stuttgart, 627 pp.2011.
Grathwohl, P., Rügner, H., Wöhling, T., Osenbrück, K., Schwientek, M., Gayler, S., Wollschläger, U., Selle, B., Pause, M., Delfs, J.-O., Grzeschik, M., Weller, U., Ivanov, M., Cirpka, O. A., Maier, U., Kuch, B., Nowak, W., Wulfmeyer, V., Warrach-Sagi, K., Streck, T., Attinger, S., Bilke, L., Dietrich, P., Fleckenstein, J. H., Kalbacher, T., Kolditz, O., Rink, K., Samaniego, L., Vogel, H.-J., Werban, U., and Teutsch, G.: Catchments as reactors: a comprehensive approach for water fluxes and solute turnover, Environmental Earth Sciences, 69, 317-333, 10.1007/s12665-013-2281-7, 2013.
Hansen, J. I., Henriksen, K., and Blackburn, T. H.: Seasonal Distribution of Nitrifying Bacteria and Rates of Nitrification in Coastal Marine Sediments, Microbial Ecology, 7, 297-304, 1981.
Hefting, M., Clément, J. C., Dowrick, D., Cosandey, A. C., Bernal, S., Cimpian, C., Tatur, A., Burt, T. P., and Pinay, G.: Water table elevation controls on soil nitrogen cycling in riparian wetlands along a European climatic gradient, Biogeochemistry, 67, 113-134, 10.1023/B:BIOG.0000015320.69868.33, 2004.
Hergert, G. W., Ferguson, R. B., Shapiro, C. A., Penas, E. J., and Anderson, F. B.: Classical Statistical and Geostatistical Analysis of Soil Nitrate-N Spatial Variability, in: Site-Specific Management for Agricultural Systems, ASA, CSSA, and SSSA Books, 175-186, https://doi.org/10.2134/1995.site-specificmanagement.c13, 1995.
Horton, R. M., Mankin, J. S., Lesk, C., Coffel, E., and Raymond, C.: A Review of Recent Advances in Research on Extreme Heat Events, Current Climate Change Reports, 2, 242-259, 10.1007/s40641-016-0042-x, 2016.
Jarvis, N., Koestel, J., and Larsbo, M.: Understanding Preferential Flow in the Vadose Zone: Recent Advances and Future Prospects, Vadose Zone Journal, 15, vzj2016.2009.0075, https://doi.org/10.2136/vzj2016.09.0075, 2016.
Jarvis, P., Rey, A., Petsikos, C., Wingate, L., Rayment, M., Pereira, J., Banza, J., David, J., Miglietta, F., Borghetti, M., Manca, G., and Valentini, R.: Drying and wetting of Mediterranean soils stimulates decomposition and carbon dioxide emission: the "Birch effect"†, Tree Physiology, 27, 929-940, 10.1093/treephys/27.7.929, 2007.
Kelly, B. P. and Pomes, M. L.: Preferential Flow and Transport of Nitrate and Bromide in Clay pan Soil, Groundwater, 36, 484-494, https://doi.org/10.1111/j.1745-6584.1998.tb02820.x, 1998.
Khan, S. U., Hooda, P. S., Blackwell, M. S. A., and Busquets, R.: Microbial Biomass Responses to Soil Drying-Rewetting and Phosphorus Leaching, Frontiers in Environmental Science, 7, 10.3389/fenvs.2019.00133, 2019.
Kuzyakov, Y. and Blagodatskaya, E.: Microbial hotspots and hot moments in soil: Concept & review, Soil Biology and Biochemistry, 83, 184-199, https://doi.org/10.1016/j.soilbio.2015.01.025, 2015.
Lair, G. J., Zehetner, F., Fiebig, M., Gerzabek, M. H., van Gestel, C. A. M., Hein, T., Hohensinner, S., Hsu, P., Jones, K. C., Jordan, G., Koelmans, A. A., Poot, A., Slijkerman, D. M. E., Totsche, K. U., Bondar-Kunze, E., and Barth, J. A. C.: How do long-term development and periodical changes of river-floodplain systems affect the fate of contaminants? Results from European rivers, Environmental Pollution, 157, 3336-3346, https://doi.org/10.1016/j.envpol.2009.06.004, 2009.
Lennon, J. T., Muscarella, M. E., Placella, S. A., and Lehmkuhl, B. K.: How, When, and Where Relic DNA Affects Microbial Diversity, mBio, 9, 10.1128/mbio.00637-00618, 10.1128/mbio.00637-18, 2018.
Mansfeldt, T.: In situ long-term redox potential measurements in a dyked marsh soil, Journal of Plant Nutrition and Soil Science, 166, 210-219, https://doi.org/10.1002/jpln.200390031, 2003.
Martin, S., Klingler, S., Dietrich, P., Leven, C., and Cirpka, O. A.: Structural controls on the hydrogeological functioning of a floodplain, Hydrogeology Journal, 28, 2675-2696, 10.1007/s10040-020-02225-8, 2020.
Moche, M., Gutknecht, J., Schulz, E., Langer, U., and Rinklebe, J.: Monthly dynamics of microbial community structure and their controlling factors in three floodplain soils, Soil Biology and Biochemistry, 90, 169-178, https://doi.org/10.1016/j.soilbio.2015.07.006, 2015.
Nimmo, J. R.: The processes of preferential flow in the unsaturated zone, Soil Science Society of America Journal, 85, 1-27, https://doi.org/10.1002/saj2.20143, 2021.
Perkins, S. E., Alexander, L. V., and Nairn, J. R.: Increasing frequency, intensity and duration of observed global heatwaves and warm spells, Geophysical Research Letters, 39, https://doi.org/10.1029/2012GL053361, 2012.
Pjevac, P., Schauberger, C., Poghosyan, L., Herbold, C. W., van Kessel, M. A. H. J., Daebeler, A., Steinberger, M., Jetten, M. S. M., Lücker, S., Wagner, M., and Daims, H.: AmoA-Targeted Polymerase Chain Reaction Primers for the Specific Detection and Quantification of Comammox Nitrospira in the Environment, Frontiers in Microbiology, 8, 10.3389/fmicb.2017.01508, 2017.
Rinklebe, J., and Langer, U.: Microbial diversity in three floodplain soils at the Elbe River (Germany), Soil Biology and Biochemistry, 38, 2144-2151, https://doi.org/10.1016/j.soilbio.2006.01.018, 2006.
Saetre, P. and Stark, J. M.: Microbial dynamics and carbon and nitrogen cycling following re-wetting of soils beneath two semi-arid plant species, Oecologia, 142, 247-260, 10.1007/s00442-004-1718-9, 2005.
Sánchez Pérez, J. M., Antiguedad, I., Arrate, I., Garci, x, a-Linares, C., and Morell, I.: The influence of nitrate leaching through unsaturated soil on groundwater pollution in an agricultural area of the Basque country: a case study, Science of The Total Environment, 317, 173-187, https://doi.org/10.1016/S0048-9697(03)00262-6, 2003.
Schimel, J., Balser, T. C., and Wallenstein, M.: MICROBIAL STRESS RESPONSE PHYSIOLOGY AND ITS IMPLICATIONS FOR ECOSYSTEM FUNCTION, Ecology, 88, 1386-1394, https://doi.org/10.1890/06-0219, 2007.
Schimel, J. P.: Life in Dry Soils: Effects of Drought on Soil Microbial Communities and Processes, Annual Review of Ecology, Evolution, and Systematics, 49, 409-432, 10.1146/annurev-ecolsys-110617-062614, 2018.
Schlögl, J., Wimmer, B., Cramaro, L., Wirsching, J., Poll, C., Pagel, H., Kandeler, E., Huhn, C., Griebler, C., Stumpp, C., and Haderlein, S. B.: Heavy rainfall following a summer drought stimulates soil redox dynamics and facilitates rapid and deep translocation of glyphosate in floodplain soils, Environmental Science: Processes & Impacts, 24, 825-838, 10.1039/D1EM00527H, 2022.

Schwientek, M., Osenbrück, K., and Fleischer, M.: Investigating hydrological drivers of nitrate export dynamics in two agricultural catchments in Germany using high-frequency data series, Environmental Earth Sciences, 69, 381-393, 10.1007/s12665-013-2322-2, 2013.
Tian, Y., Schindlbacher, A., Malo, C. U., Shi, C., Heinzle, J., Kwatcho Kengdo, S., Inselsbacher, E., Borken, W., and Wanek, W.: Long-term warming of a forest soil reduces microbial biomass and its carbon and nitrogen use efficiencies, Soil Biology and Biochemistry, 184, 109109, https://doi.org/10.1016/j.soilbio.2023.109109, 2023.
Tournier, E., Amenc, L., Pablo, A. L., Legname, E., Blanchart, E., Plassard, C., Robin, A., and Bernard, L.: Modification of a commercial DNA extraction kit for safe and rapid recovery of DNA and RNA simultaneously from soil, without the use of harmful solvents, MethodsX, 2, 182-191, https://doi.org/10.1016/j.mex.2015.03.007, 2015.
Unger, S., Máguas, C., Pereira, J. S., David, T. S., and Werner, C.: The influence of precipitation pulses on soil respiration – Assessing the "Birch effect" by stable carbon isotopes, Soil Biology and Biochemistry, 42, 1800-1810, https://doi.org/10.1016/j.soilbio.2010.06.019, 2010.
Veach, A. M. and Zeglin, L. H.: Historical Drought Affects Microbial Population Dynamics and Activity During Soil Drying and Re-Wet, Microbial Ecology, 79, 662-674, 10.1007/s00248-019-01432-5, 2020.
Venterink, H. O., Wiegman, F., Van der Lee, G. E. M., and Vermaat, J. E.: Role of Active Floodplains for Nutrient Retention in the River Rhine, Journal of Environmental Quality, 32, 1430-1435, https://doi.org/10.2134/jeq2003.1430, 2003.
Vos, M., Wolf, A. B., Jennings, S. J., and Kowalchuk, G. A.: Micro-scale determinants of bacterial diversity in soil, FEMS Microbiology Reviews, 37, 936-954, 10.1111/1574-6976.12023, 2013.
Wassenaar, L. I., Hendry, M. J., Chostner, V. L., and Lis, G. P.: High Resolution Pore Water δ2H and δ18O Measurements by H2O(liquid)−H2O(vapor) Equilibration Laser Spectroscopy, Environmental Science & Technology, 42, 9262-9267, 10.1021/es802065s, 2008.
Wirsching, J., Wimmer, B., Ditterich, F., Schlögl, J., Martin-Laurent, F., Huhn, C., Haderlein, S., Kandeler, E., and Poll, C.: 13C assimilation as well as functional gene abundance and expression elucidate the biodegradation of glyphosate in a field experiment, Environmental Pollution, 306, 119382, https://doi.org/10.1016/j.envpol.2022.119382, 2022.

Appendices

Appendix A: Soil profile in a soil core from the Ammer valley

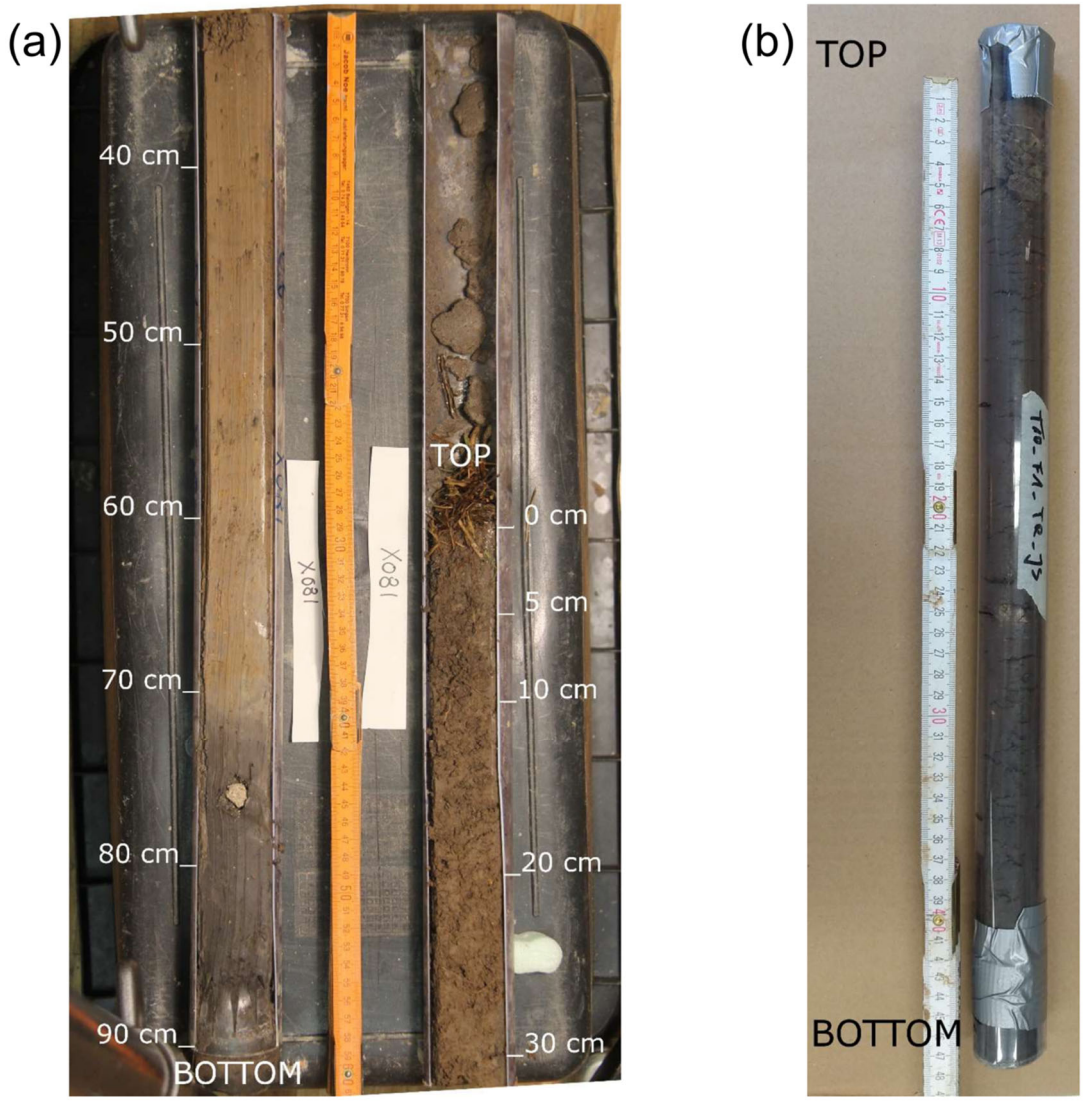


Figure A1: (a) Photo of the upper 90 cm soil profile from a location 100 m NW' of the study site. A 1.20 m deep core was retrieved with a direct push probe (6610 DT, Geoprobe, Salina, Kansas, US), the core was cut in two parts lengthwise for better visibility of the sediments and crosswise at 0.6 m for taking the photo. The missing 30 cm are due to core loss at the bottom of the core. Depth in cm below ground level is depicted besides the core. The upper 70 cm of the core are of uniform red-brown color until at 71 cm the color abruptly changes to grey marking the transition from the Go to the Gr horizon in this Gleysol. Maximum sampling depth of the presented study was 50 cm, which was well within the Go horizon. (The photo is courtesy of S. Klingler and S. Martin.) (b) Photo of a 50 cm soil core from the presented study (plot D1). The uniform red-brown color is visible through the plastic liner. (Figure reproduced from Schlögl et al. (2022) with permission from the Royal Society of Chemistry.)

Appendix B: Soil organic matter

Determination of total organic carbon (TOC)

For the analysis of soil organic matter as total organic carbon (TOC), cores from plots D1–3 (Day 10) and from W1–3 (Day 14) were cut into the following segments: 0–5 cm depth, 5–15 cm, 15–25 cm, 25–35 cm, 35–45 cm, 45–50 cm. The corresponding depth segments from all D plots and from all W plots, respectively, were combined and aliquots of 10 g of soil were freeze-dried (CHRIST ALPHA 1-4, CHRIST, Germany) and were ground to a grain size of < 63 µm with a planetary ball mill. One 1 g aliquot of each sample was decalcified with 16 % aqueous HCl and subsequently washed with ultrapure

water until reaching at minimum a pH of 5. The sample was again dried and then weighed to determine the amount of inorganic carbon. Inorganic carbon was independently determined by acid titration of a second subsample to ascertain the decalcification. The dried and decalcified subsample was analyzed for TOC in an elemental analyzer (Elementar vario EL, Elementar, Hanau, Germany) with four replicate measurements per sample. TOC was then normalized to the initial dry weight of the sample and expressed as weight%.

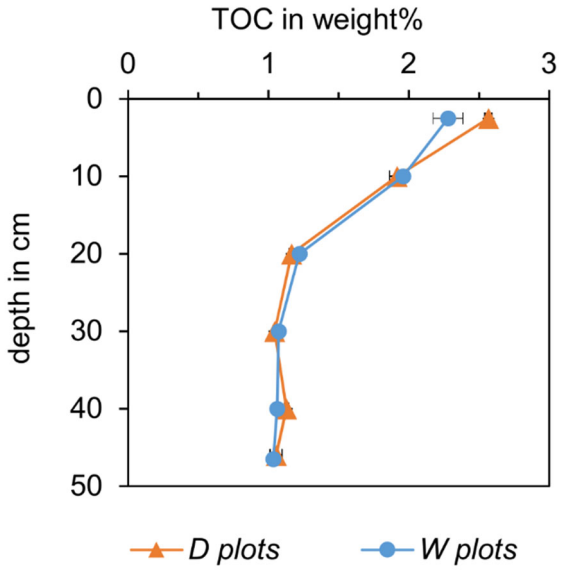


Figure B1: Distribution of soil organic carbon (as TOC) in weight% in a 50 cm depth profile of the studied Gleysol on irrigated plots after 14 days of irrigation (W plots, blue dots) and dry control plots (D plots, orange triangles). (Figure reproduced from Schlögl et al. (2022) with permission from the Royal Society of Chemistry.)

Appendix C: Soil texture

Determination of soil texture

For the analysis of grain size distribution, cores from plots D1–3 (Day 10) and from W1–3 (Day 14) were cut into the following segments: 0–5 cm depth, 5–15 cm, 15–25 cm, 25–35 cm, 35–45 cm, 45–50 cm. The corresponding depth segments from all D plots and from all W plots, respectively, were combined. For each depth segment, grain size analysis was conducted following the German Standard (Din deutsches institut für normung e. v., 2017). Aliquots of 50 g per sample were sieved wet through sieves of 2 mm, 1 mm and 125 µm mesh size to separate the fraction smaller than 125 µm. The fraction bigger than 125 µm was dried and sieved dry through sieves of 500 µm, 250 µm, and 125 µm. The fraction smaller than 125 µm was further analyzed by sedimentation analysis using the integral suspension pressure method (ISP) (Durner et al., 2017) using a PARIO device (Meter Group, Munich, Germany).

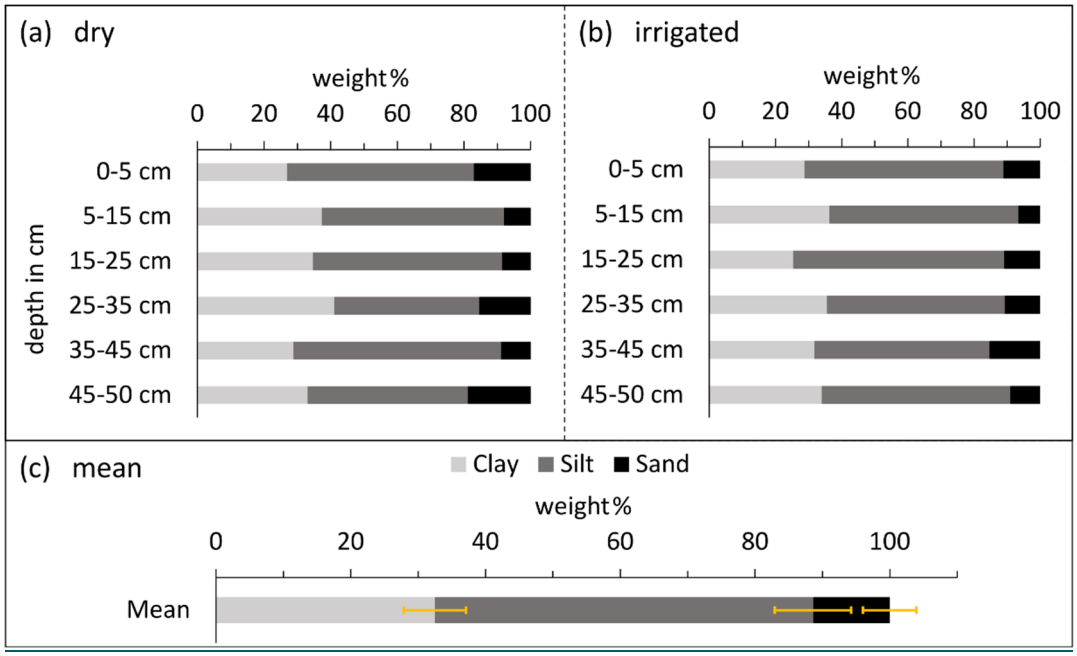


Figure C1: Grain size distribution in weight% of clay (light grey), silt (dark grey), and sand (black). (a) and (b). Grain size distribution in 50 cm soil profiles of the studied Gleysol on dry control plots (a) and irrigated plots (b). (c). Mean values and standard deviations (yellow bars) of the grain size distribution calculated from all samples and depths from dry and irrigated plots (n = 12). The soil is a silty clay loam. (Figure reproduced from Schlögl et al. (2022) with permission from the Royal Society of Chemistry.)

Appendix D: Weather data

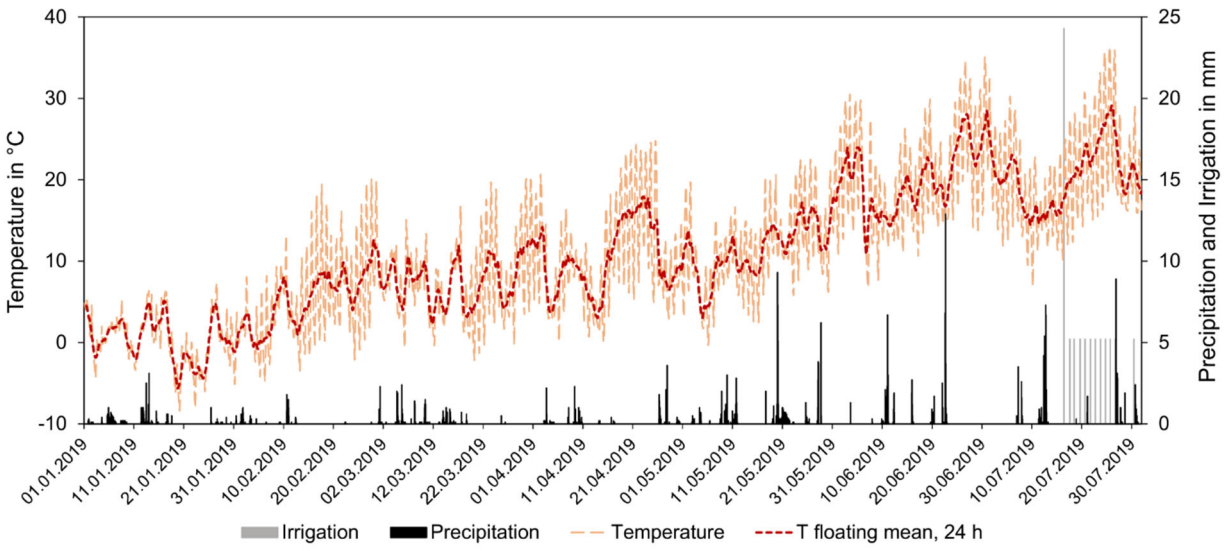


Figure D1: Hourly data of temperature (T) in °C (light red line), natural precipitation (black bars) and irrigation (grey bars) in mm and a 24 h floating mean of the temperature in °C for the period from 1 January 2019 until 31 July 2019 from the weather station in Tübingen-Unterjesingen. The experiment took place from 16 July 2019 until 30 July 2019. (Figure reproduced from Schlögl et al. (2022) with permission from the Royal Society of Chemistry)

Appendix E: Calculation of reference evapotranspiration ETo

The reference evaporation ETo was calculated according to FAO Irrigation and Drainage Paper No. 56 (Allen et al., 1998).

Table E1: Data on temperature (T), relative humidity (RH) and global radiation (Rs) from the weather station in Tübingen-Unterjesingen used for the calculation of the reference evapotranspiration ETo for the period 1 to 31 July 2019

Parameter	Measured value
T_{max} in °C	36.3
T_{mean} in °C	20.4
T_{min} in °C	6.9
RH_{max} in %	100.0
RH_{mean} in %	68.7
RH_{min} in %	26.0
Rs in W m^{-2}	236.0
ETo in mm day^{-1}	4.2

Appendix F: Gravimetric soil water content

The methodology is described in the main text.

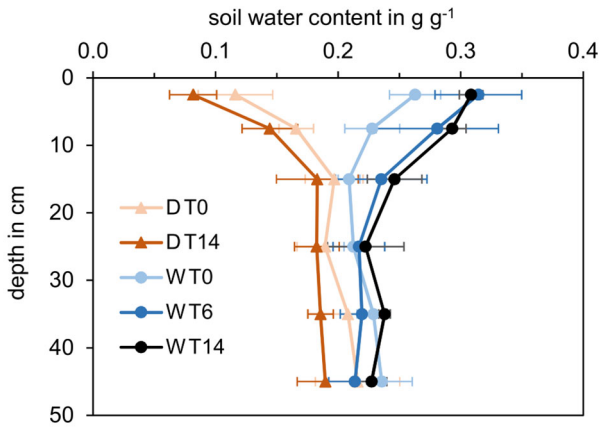


Figure F1: Gravimetric oil water content in g g^{-1} on Dry (D) and irrigated (W) plots on Days 0, 6 and 14 (T0, T, T14). Mean values and standard deviations of replicates from three experimental plots are shown. (Figure reproduced from Schlögl et al. (2022) with permission from the Royal Society of Chemistry)

Appendix G: Microbial community analysis

Relative sequence abundance

The methodology is described in the main text.

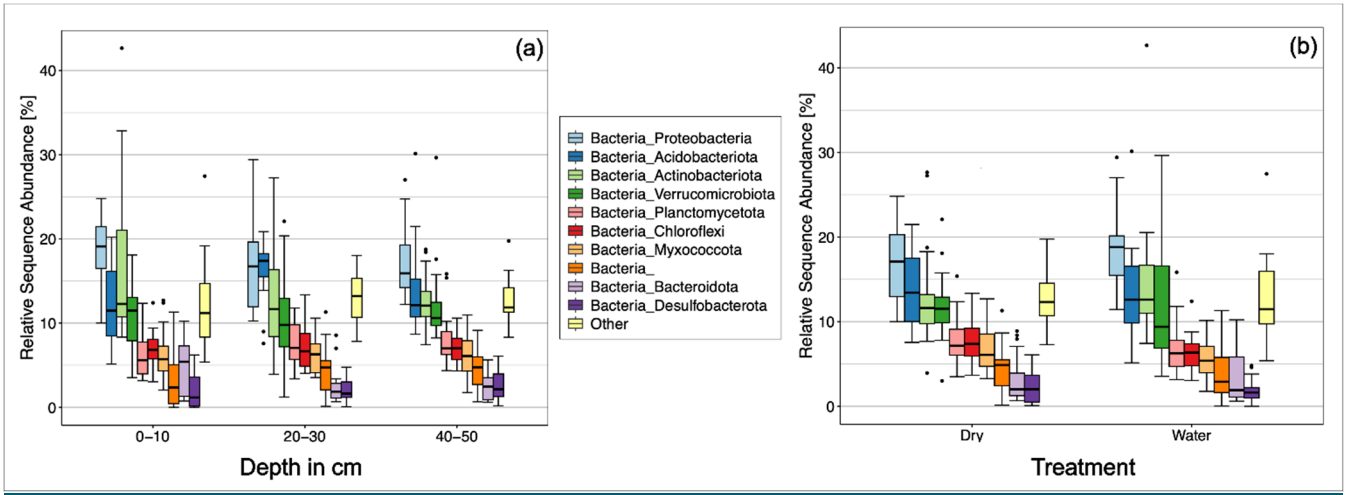


Figure F1: Relative sequence abundance of bacteria phyla in the studied soil sorted by depth (a) and treatment (b).

Appendix H: Coefficients of variation of nitrate and ammonium masses on W plots

Coefficients of variation were calculated from mean values and standard deviations (n = 3) of nitrate and ammonium masses along the soil profile.

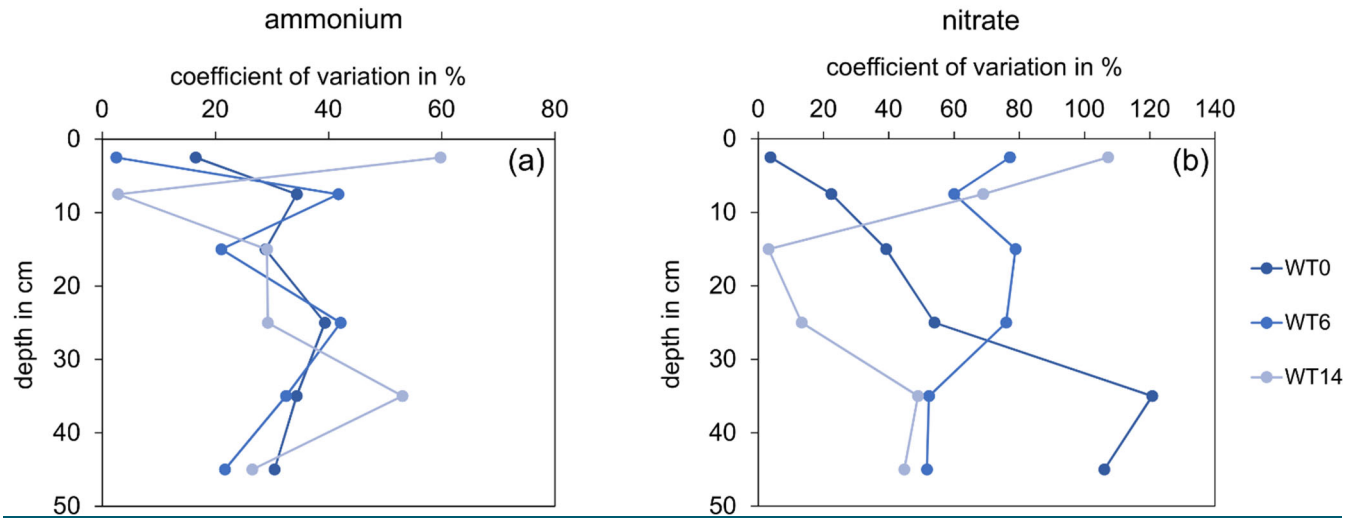


Figure G1: Coefficients of variation of ammonium (a) and nitrate (b) masses on W plots at Days T0, T6 and T14.

Appendix I: Calculation atmospheric ammonium-N deposition

The atmospheric ammonium-N deposition on the cross-sectional area of an experimental soil core was calculated to evaluate potential sources of ammonium increase observed in the topsoil. Weekly atmospheric ammonium fluxes averaged over one year were taken from Beyn et al. (2014).

Table H1: Calculation of the atmospheric ammonium-N deposition on the cross-sectional area of a soil core with a diameter of 3.5 cm within one week.

Atmospheric ammonium-flux average over one year in µM ammonium m^{-2} per week	Source: Beyn et al. 2014
wet deposition	752
dry deposition	66.7
total	818.7
Molar mass	
M(ammonium) in g mol^{-1}	18.0386
M(N) in g mol^{-1}	14.007
cross sectional area sample core in m^2	0.000962
total ammonium-flux average over one year	
in µg ammonium m^{-2} per week	14768.20
in mg ammonium m^{-2} per week	14.77
in µg ammonium-N m^{-2} per week	11467.53
in mg ammonium-N m^{-2} per week	11.47
on cross-sectional area of a sample core	
in mg ammonium-N per week	0.01103

Appendix J: Calculation atmospheric nitrate-N deposition

The atmospheric nitrate-N deposition on the cross-sectional area of an experimental soil core was calculated to evaluate potential sources of nitrate increase observed in the topsoil. Weekly atmospheric nitrate fluxes averaged over one year were taken from Beyn et al. (2014).

Table I1: Calculation of the atmospheric nitrate-N deposition on the cross-sectional area of a soil core with a diameter of 3.5 cm within one week.

Atmospheric nitrate-flux average over one year in µM nitrate m^{-2} per week	Source: Beyn et al. 2014
wet deposition	468.9
dry deposition	60.6
total	529.5
Molar mass	
M(nitrate) in g mol^{-1}	61.977
M(N) in g mol^{-1}	14.007
cross sectional area sample core in m^2 (radius = 3.5 cm)	0.000962
total nitrate-flux average over one year	
in µg nitrate m^{-2} per week	32816.82
in mg nitrate m^{-2} per week	32.82
in µg nitrate-N m^{-2} per week	7416.71
in mg nitrate-N m^{-2} per week	7.42
on the cross-sectional area of a sample core	
in mg nitrate-N per week	0.0071